PSFC/JA-00-25

X-ray Observations of 2l-nl′ Transitions and Configuration Interaction Effects from Kr, Mo, Nb and Zr in Near Neonlike Charge States from Tokamak Plasmas

J.E. Rice, K.B. Fournier[1], J.A. Goetz, E.S. Marmar, J.L. Terry

September 2000

Plasma Science and Fusion Center
Massachusetts Institute of Technology
Cambridge, MA 02139 USA

[1]Lawrence Livermore National Laboratory, P.O. Box 808, L-41, Livermore, CA 94551.

This work was supported by the U.S. Department of Energy, Cooperative Grant No. DE-FC02-99ER54512. Reproduction, translation, publication, use and disposal, in whole or in part, by or for the United States government is permitted.

Submitted for publication to *Journal of Physics B.*

X-ray Observations of 2l − nl′ Transitions and Configuration Interaction Effects from Kr, Mo, Nb and Zr in Near Neonlike Charge States from Tokamak Plasmas

J. E. Rice, K. B. Fournier†, J. A. Goetz, E. S. Marmar and J. L. Terry

Plasma Science and Fusion Center, MIT, Cambridge, MA 02139-4307

†*Lawrence Livermore National Laboratory, P. O. Box 808, L-41 Livermore, CA 94551*

(September 7, 2000)

Abstract

X-ray spectra of $2l - 3l'$ transitions in the elements krypton (Z=36), zirconium (Z=40), niobium (Z=41) and molybdenum (Z=42) from charge states around neonlike have been observed from Alcator C and Alcator C-Mod plasmas. Accurate wavelengths (± .5 mÅ) have been determined in reference to neighboring aluminum, silicon, sulphur, chlorine and argon lines with relatively well known wavelengths. Line identifications have been made by comparison to *ab initio* atomic structure calculations, using a fully relativistic, parametric potential code. Calculated wavelengths and oscillator strengths are presented for $2l - 3l'$ transitions in neonlike ions and neighboring Na-, Mg-, F- and O-like satellites. Electric quadrupole transitions in neonlike ions of the form 2s − 3d and 2p − 3p are found to be relatively bright, and their measured intensities agree well with the results of collisional-radiative modeling. The 2p − 3s magnetic quadrupole transition is also relatively intense in the absence of collisional de-excitation at tokamak densities (10^{13}-10^{15}/cm^3). For krypton, transitions with upper levels up to n=9 have been observed, and

the measured wavelengths and intensities have been compared with calculations. For some neonlike transitions with nearly degenerate upper levels, there can be substantial configuration interaction which alters the line intensities.
32.30.Rj 34.80.Dp 52.55.Fa

I. INTRODUCTION

There has been considerable interest in x-ray transitions from high Z atoms with charge states around the neonlike isosequence, attained in pulsed power [1–4], tokamak [5–10] and laser produced [11–13] plasmas. X-ray lasing [14,15] has been demonstrated in neonlike ions, and a need to understand the kinetics of this system has motivated development of very precise collisional-radiative modeling tools [16]. The identifications of many x-ray lines from neonlike ions allow high resolution experimental data to be used for benchmarking multi-electron atomic structure calculations [17–21,7–9]. Collisional radiative modeling of line intensities from neon-, fluorine-, sodium- and magnesiumlike ionization states has demonstrated the importance of excitation-autoionization in overall charge state balance in tokamak plasmas [22]. Rates for this process, in conjunction with the latest dielectronic recombination rates [23], have led to a reassessment of the importance of molybdenum radiation in energy balance [24] in tokamak plasmas. Most of the work that has been done in the past has been limited to $3-3$, $2-3$ and $2-4$ transitions in the Ne-I iso-electronic sequence and adjacent charge states. Recently, high n lines in neonlike iron have been measured for application to astrophysical data [25]. High temperature, optically thin tokamak plasmas enable the measurement of many lines originating in transitions from levels having $n \geq 5$; in fact, all of the transitions in the $2p-nd$ series in Mo^{32+} lying under the ionization potential have been measured [8].

The availability of a large number of transitions in several adjacent elements provides the opportunity to study the systematics of configuration interaction (CI) effects [9]. The present work demonstrates numerous instances of different transitions that are enhanced or suppressed by CI. It has also been observed [7–9] that a systematic uncertainty enters the calculation for the wavelengths of transitions with a 2s hole in the upper level through the treatment of QED contributions in the calculation of these level energies. The same discrepancy is noted in the present work for all n when a relativistic parametric potential code (RELAC [26,27]) is used for the level energies. The tendency to overestimate level

energies in multi-electron atoms based on hydrogenic calculations with QED corrections [28] has been noted in comparisons between precise measurements of the level structure in neonlike ytterbium [17] and calculations from other relativistic codes which use the same procedure as RELAC. Issues relating to the calculation of level energies for states with a 2s hole have been investigated based on observations of the level structure of neonlike gold [18]. Further, the spectra observed in the present work allow the study of the intensity of dipole forbidden E2 and M2 lines. These lines are potentially useful as diagnostics of local temperature and density conditions.

In this paper, measured wavelengths and brightnesses, and calculated wavelengths, line intensities and oscillator strengths for 2p − 3d, 2p − 3s, 2s − 3p, 2s − 3d and 2p − 3p transitions in the neonlike ions of Kr, Mo, Nb and Zr, in addition to associated 2p − 3s, 2p − 3d and 2s − 3p satellites from magnesium-, sodium-, fluorine- and oxygenlike ions are presented. Measured and calculated lines from higher n transitions in neonlike krypton are also presented. In Section II the experimental setup and wavelength calibration are described, and in Section III a discussion is given of the atomic structure codes used and modeling issues are outlined. In Section IV the 2 − 3 experimental results and comparison with theory are presented. This includes extensive line tables, a Z scaling of satellite wavelengths and modeling of magnetic and electric quadrupole lines. In Section V experimental results for high n ground state transitions in Kr and Mo are compared with theory, with numerous examples of configuration interaction effects being demonstrated.

II. EXPERIMENT DESCRIPTION

The x-ray observations described here were obtained from the Alcator C [29] and Alcator C-Mod [30] tokamaks. Alcator C operated from 1978-1986, with toroidal magnetic fields up to 12 T, a molybdenum poloidal limiter and with central electron density and temperature in the ranges of 5×10^{12} to $5\times10^{15}/\mathrm{cm}^3$ and 600 to 2500 eV, respectively. Alcator C-Mod is a compact high field device with all molybdenum plasma facing components. For the

measurements presented here, plasma parameters were in the range of $1.4\times10^{14}/\mathrm{cm}^3 \leq \mathrm{n}_{e0} \leq 3.4\times10^{14}/\mathrm{cm}^3$ and 1100 eV $\leq \mathrm{T}_{e0} \leq$ 3000 eV. Molybdenum is an intrinsic impurity and krypton was introduced through a piezo-electric valve in both devices. A laser blow-off impurity injection system [31], which has been utilized to study impurity transport, was used to inject niobium and zirconium into Alcator C-Mod plasmas.

The $2l - 3l'$ spectra of krypton from Alcator C were obtained with a von Hamos type spectrometer equipped with a pentaerythritol (PET) crystal (2d = 8.742 Å), and with wavelength coverage between 6 and 8 Å. The active area of the position sensitive proportional counter detector was large (12 cm), which allowed for up to 400 mÅ coverage in one wavelength setting, but non-uniformities along the length of the Be entrance window led to sensitivity variations, so some line ratios from opposite ends of the detector may be up to 25% off. The x-ray spectra from Alcator C-Mod were recorded by a five chord, independently spatially scannable, high resolution x-ray spectrometer array [32]. Four of these von Hamos type spectrometers have quartz crystals with 2d spacings of 6.687 Å, and wavelength coverage from 2.7 to 4.1 Å, 120 mÅ at a time. The remaining spectrometer has an ammonium dihydrogen phosphate (ADP) crystal with a 2d spacing of 10.640 Å, and a wavelength range from 4.3 to 6.5 Å. Wavelength calibration [5–9] has been achieved by determining the instrumental dispersions in reference to H- and He-like argon, chlorine, sulphur, silicon and aluminum lines and previously measured molybdenum [8] lines. The argon was introduced through a piezo-electric valve and chlorine and sulphur are intrinsic impurities. Si and Al were also injected into Alcator C plasmas with a laser blow-off system. Lines from hydrogen- [33,34] and helium-like [35–37] charge states are taken to have well known wavelengths, either measured or calculated. Experimental wavelengths were determined by performing a least squares fit to observed spectra using gaussian line shapes; measured line widths are dominated by Doppler broadening. The wavelengths of the H- and He-like calibration lines were taken to have an uncertainty of $\pm$ 0.1 mÅ. For the $2 - 3$ spectra of krypton, a quadratic fit was performed for the experimental dispersions, using an iterative procedure for neighboring spectra, whereas for all other transitions, a linear dispersion was determined. Overall

accuracy of experimental wavelengths in the Tables is ± 0.5 mÅ, although for spectra with good statistics and several calibration lines, the accuracy is ± 0.3 mÅ.

III. CALCULATION OF ENERGY LEVELS, OSCILLATOR STRENGTHS AND LINE INTENSITIES

Ab initio atomic structure calculations for the aluminum- through oxygenlike isosequences (ground states $2p^6 3s^2 3p$ to $2s^2 2p^4$, respectively) have been performed using the fully relativistic RELAC code [26,27]. RELAC solves the Dirac equation by optimizing a parametric potential in order to minimize the average energies of a set of user specified configurations. Because a different potential is found for each set of configurations, the calculations are not rigorously self-consistent. For each set of configurations in the problem, the fine structure level energies are then computed in intermediate coupling on jj-coupled basis functions. Contributions to level energies from the Breit operator and vacuum polarization effects [38] are also computed. RELAC computes the self-energy of a bound electron due to the emission and re-absorption of a virtual photon by determining an effective Z which satisfies the requirement that the expectation value of the relativistic subshell $< r_{nlj} >$ agrees with the corresponding hydrogenic value and then, in the case of an s- or p-orbital, interpolating the result on the hydrogenic values tabulated in Ref. [28]. In a previous paper that discussed the structure of neonlike molybdenum ions [8], part of the systematically larger difference between observed and calculated 2s − np transition energies and the more accurately predicted 2p − nd transition energies was ascribed to RELAC's use of the effective Z method for QED corrections to the binding energies of L-shell electrons. Further, the assumption of a point nucleus (rather than a finite nuclear charge distribution) introduces a systematic error in the calculated wave functions for orbitals with large probability near r=0. A quantitative discussion of the observed and calculated 2s − 3p neonlike transition energies is given below.

Synthetic spectra were calculated for each ion in the present work using the HULLAC

atomic physics package. The energy levels and radiative transitions rates (for electric and magnetic dipole and quadrupole transitions: E1, M1, E2 and M2) [39], along with autoionization rates [40], are calculated by RELAC. All levels with principal quantum number n $\leq$ 10 have been allowed to interact in the calculation of the structure and rates for each ion. Electron impact excitation collision cross sections between all levels of each ion are computed semi-relativistically in the distorted wave approximation using RELAC's multi-configuration wave functions. The rapid calculation of so many collision strengths is made possible by the factorization theorem and interpolation of radial integrals technique of Bar-Shalom, Klapisch and Oreg [41]. Collisional excitation rate coefficients γ are found by averaging the collisional cross sections $< v\sigma(v) >$ over a Maxwellian velocity distribution. All level energies and rate coefficients have been entered into the collisional-radiative (CR) rate matrix for the ions of each element, and the resulting steady state level populations are then found according to

$$\frac{dn_j}{dt} = 0 = \sum_{i \neq j} n_i R_{i,j} - n_j \sum_{i \neq j} R_{j,i} \tag{1}$$

where n_j is the population in level j, and $R_{i,j}$ is the rate at which population leaves level i and goes to level j, possibly belonging to a neighboring ion. (Rates R are related to rate coefficients γ by $R_{j,i} = n_e \gamma_{j,i}$ where n_e is the electron density.) The resulting intensity for an observed line is given by

$$I_{j,i} = n_j A_{j,i} \tag{2}$$

where $A_{j,i}$ is the radiative transition rate for some multipole. Thus, for levels connected to the ground only by slow (non-electric dipole) decays, the resulting emission can be strong if the upper level's population is large. Examples of bright E2 and M2 lines will be discussed below. These lines are sensitive to increasing electron density through the competition between radiative decays and collisional destruction of the upper level. For the high atomic number elements studied here, the critical densities above which collisions suppress the observed emission are higher than can be achieved in tokamak plasmas.

RELAC's wavefunctions are computed taking full account of CI between levels with the same parity and the same total angular momentum. The result is that the physical state

of the upper and lower level in each observed transition can have components from many configurations. The CI can have many effects on an ion's spectrum: in the case of Na- and F-like ions, classically forbidden transitions involving two jumping electrons are enabled (see, for example, Table III). Also, when two interacting levels become closely separated in energy, strength is transferred from one transition (potentially quenching it fully) to the other [42,43]. Three measured examples of this phenomenon on strong lines in the neonlike spectra of Kr and Mo are presented in § 5, below. The strength of a line is defined as the square of the reduced dipole matrix element

$$S = |\langle\psi\| \sum_i \vec{\mathrm{r}}_i \|\psi'\rangle|^2 \tag{3}$$

where ψ (ψ') are the physical wavefunctions composed of many basis-states, the sum runs over all N electrons of the atom (or ion) and r_i is the radial position of the i^{th} electron in Bohr units. S is related to the radiative decay rate according to

$$g_u A_{u,l} = \frac{64\pi^4 e^2 \mathrm{a}_0^2}{3h} S\sigma^3 \tag{4}$$

where g_u is the statistical weight of the upper level of the transition, a_0 is the Bohr radius and σ is the wave number of the spectral line in cm^{-1}. The ultimate contribution of each basis component to the matrix element in eq. 3 is determined by the product of the the mixing coefficient (with a definite phase) and the radial transition integral involving one-electron orbital functions

$$\langle nlj\|\vec{\mathrm{r}}\|n'l'j'\rangle = (-1)^l[(2l+1)(2l'+1)]^{1/2} \times \begin{pmatrix} l & 1 & l' \\ 0 & 0 & 0 \end{pmatrix} \int_0^\infty r P_{nl} P_{n'l'} dr. \tag{5}$$

The superposing of positive and negative terms in eq. 3 can result in constructive or destructive interference, thus transferring line strength from one transition to another [42,43]. Hence, no general statement can be made about the direction of the strength transfer (i.e. from lower to higher energy levels) and the full multiconfiguration calculation must be done in each case.

IV. 2 − 3 EXPERIMENTAL SPECTRA AND INTERPRETATION

Shown in Fig. 1 is the 2 − 3 spectrum of neonlike krypton (Kr^{26+}), with satellites; previous observations can be found in Refs. [2,3,12,13]. This is a composite spectrum obtained by scanning in wavelength during a sequence of reproducible Alcator C discharges, with a peak electron density of $2.6\times10^{14}/cm^3$ and a peak electron temperature of 1450 eV. The spectrum is dominated by the neonlike electric-dipole transitions 3C ($2p_- - 3d_-$) and 3D ($2p_+ - 3d_+$). (The standard notation for Ne-like transitions [44] is used.) The 3F and 3G ($2p_\mp - 3s_+$) transitions, including the magnetic quadrupole line (M2, $2p_+ - 3s_+$, ΔJ=2) at 7519.2 mÅ, are also intense. Transitions with a 2s hole (3A, $2s - 3p_+$ and 3B, $2s - 3p_-$) are bright, including the electric quadrupole $2s - 2d_+$ line at 6103.8 mÅ. Also apparent are F-, Na- and Mg-like satellites. This composite spectrum is comprised of 6 individual spectra from different discharges, and considering non-uniformities along the detector (as mentioned above), the relative intensities of lines separated by more than 150 mÅ have a 25% uncertainty. Shown in the bottom of Fig.1 is a synthetic spectrum, which is in good qualitative agreement. Transition designations, experimental and theoretical wavelengths and calculated oscillator strengths for all of these lines are presented in Tables I-IV. Most observed transitions are within 3 mÅ of the calculated wavelengths, or about 0.04%. The synthetic spectrum was computed for T_e = 1600 eV and $n_e = 1.0\times10^{14}/cm^3$. An expanded view of this spectrum in the vicinity of the 3C transition at 6697.3 mÅ, which was obtained during a single discharge, is shown in Fig.2. Several bright Na-like satellites are present, along with a Mg-like transition, on the long-wavelength side; on the short-wavelength side are several less intense F-like satellites. The calculated spectrum is overlaid, and in good agreement (see Tables I-IV). The helium-like Si^{12+} resonance and forbidden lines used for the wavelength calibration are indicated by the vertical dotted lines.

The neonlike 3C spectrum and long-wavelength satellites have been obtained for several row 5 transition metals [4,12]. A comparison of these spectra is shown in Fig. 3, and all are qualitatively similar. (The Pd lines were previously reported [9,45].) This allows

for the study of relative satellite transition wavelengths as a function of atomic number. Transition designations, experimental and theoretical wavelengths and calculated oscillator strengths for neonlike $2l - 3l'$ lines, along with nearby satellites, are given in Tables V-VII for molybdenum, niobium and zirconium. These wavelengths may be compared to previous measurements [4,5,12]; in Ref. [5], wavelengths of the Cl and S calibration lines were only given to the nearest mÅ, and were based on older, less accurate calculations; in Ref. [4] there were significant Doppler shifts due to the expanding source, leading to substantial uncertainties in the measured wavelengths; in Ref. [12] there was no independent wavelength calibration and all lines were given in reference to the calculated neonlike 3C and 3D lines. Shown in Fig. 4 are the measured wavelength differences between the 3C resonance lines and the three brightest satellites considered, the $2p_- - 3d_-$ J=$\frac{1}{2}$ sodiumlike transition, the $2p_- - 3d_-$ J=$\frac{3}{2}$ sodiumlike transition and the $2p_- - 3d_-$ J=1 magnesiumlike transition (normalized to the resonance line wavelength),

$$(\lambda_{3C} - \lambda_{sat})/\lambda_{3C} \tag{6}$$

as a function of the atomic charge of the neonlike ion. There is a systematic trend for the satellites to approach the neonlike line in wavelength for higher atomic number, for the three brightest satellites considered. This trend is also apparent in the calculations, as shown by the solid lines in Fig. 4. The Mg-like Pd line at 3763.6 mÅ was mistakenly identified with the unclassified feature at 3774.6 mÅ in Table V of Ref. [9].

As is apparent from Fig. 1, the ΔJ=2 $2p_+ - 3s_+$ magnetic quadrupole (M2) transition in krypton at 7519.2 mÅ is quite prominent, although the radiative transition rate, relative to the nearby ΔJ=1 $2p_+ - 3s_+$ electric-dipole transition (3G) at 7504.4 mÅ, is six orders of magnitude slower (5.4×10^6 versus 5.3×10^{12} s^{-1}) while the collisional excitation rates coefficients from the ground level are within a factor of two (1.3×10^{10} versus 3.0×10^{10} cm^{-3} s^{-1}). The intensity of this transition is enhanced in the collisional radiative model by a build-up of population in the nearly metastable upper level. The corresponding transition in molybdenum is similarly bright, as can be seen in Fig. 5. Central plasma parameters for the

molybdenum spectrum were $T_e = 1800$ eV and $n_e = 1.8\times10^{14}/cm^3$. The predicted intensities of these magnetic quadrupole transitions in both krypton and molybdenum are in excellent agreement with measurements relative to the nearby electric-dipole lines. The collisional radiative intensities of these lines are sensitive to the cascade channels from higher n levels in the model; 93.5% of the population in the upper level of the M2 line comes from radiative cascades through levels with $n \leq 9$, versus 88% for the upper level of 3G. (These cascades were not properly included in the synthetic spectrum of Fig. 1.) The relative intensities of the M2/3G lines may be used as an electron density diagnostic, because at higher densities, collisional de-excitation of the M2 line dominates over radiative decay. This is demonstrated in Fig.6 where this calculated line ratio is shown as a function of density for molybdenum and krypton. Also included are the measured points deduced from Fig. 5. Unfortunately, the electron density in tokamak plasmas is about an order of magnitude too low to be able to take advantage of the diagnostic application of this line ratio for these species.

Near the bright Kr^{26+} $2p_- - 3s_+$ transition 3F (7267.5 mÅ) are the $\Delta J=2$, $\Delta l=0$ electric quadrupole transitions $2p_+ - 3p_+$ (E22) and $2p_+ - 3p_-$ (E23), at 7208.1 and 7277.5 mÅ, respectively. (These transitions were seen in Ag [6].) These lines are shown in Fig. 7, along with the corresponding, and previously unreported transitions in Mo^{32+} at 5008.4 and 5072.8 mÅ, respectively. Central plasma parameters for the molybdenum spectrum were T_e = 1850 eV and $n_e = 1.6\times10^{14}/cm^3$. Also shown in Fig. 7 are synthetic spectra, again in good agreement with the observations. Similar to the magnetic quadrupole lines, these electric quadrupole lines have radiative transition rates that are at least three orders of magnitude lower than that of 3F, and yet these lines are relatively strong. Again, this is because of the highly populated nature of the upper levels of these transitions. E23 and E22 both have quadrupole transition rates to the ground level of 2.0×10^{10} s^{-1} in Mo^{32+} (relative to 7.8×10^{12} s^{-1} for 3F). The branching ratios of E23 and E22 to the ground level, as opposed to $\Delta n=0$ dipole decays to $2p^5 3s$ levels, are 0.63 and 0.34, respectively. The other related electric quadrupole transition E21 ($2p_- - 3p_+$) in molybdenum is located very close to the intense 3D transition, while in krypton it is blended with relatively bright F- and Mg-like

lines. Similarly, the relatively weak 3E transitions in Mo and Kr are blended with nearby satellites.

The ΔJ=2, Δl=2 electric quadrupole transitions (2s $-$ 3d$_+$) in Mo^{32+} and Kr^{26+}, at 4276.2 and 6103.8 mÅ, respectively, are relatively bright, in spite of their slow radiative transition rates, in a similar fashion to the 2p $-$ 3p lines. X-ray spectra in the neighborhoods of these lines are shown in Fig. 8, which also include the 2s $-$ 3p$_+$ transitions 3A. Core plasma parameters for the molybdenum spectrum were T_e = 1800 eV and n_e = 1.4×10^{14}/cm^3. The 4276.2 mÅ line wasn't observed in a previous study of the 2 $-$ 3 transitions in molybdenum because it was out of the spectral range of the instrument [5]. Shown for comparison are the simulated spectra; the calculated neonlike lines appear systematically on the short wavelength side. This shift has been noted earlier [7–9,25] and is due to a combination of factors. In the model potential, a point nucleus has been assumed instead of a distribution of charge over a finite radius, and this has a larger effect on orbitals with a large probability near r=0, like 2s. In addition, QED effects are strongest for s-orbitals and are only estimated in the calculations. The relative intensities of the neonlike lines are in fairly good agreement with the calculations, although E2s is observed to be slightly brighter than calculated relative to 3A for both molybdenum and krypton. The reason that these electric quadrupole lines are so strong in spite of their slow transition rates can be seen in the competition between the E2 channel and the allowed Δn=0 (3d$\rightarrow$3p) E1 decay channel. The branching ratios for the E2s decays are around 0.4 and 0.3 for Mo and Kr, respectively; at the relatively low densities of tokamak plasmas, these forbidden lines are quite bright.

An x-ray spectrum of molybdenum at slightly longer wavelength, for a higher temperature plasma (3000 eV) is shown in Fig. 9. This spectrum is dominated by the fluorinelike 2p$_-$ $-$ 3d$_-$ J=$\frac{5}{2}$ transition at 4498.3 mÅ. In addition to 3A and 3B, another intense line in this spectrum is the oxygenlike 2p$_+$ $-$ 3d$_+$ (J=2 to J=3) transition [10] at 4535.8 mÅ. The corresponding oxygenlike 2p$_+$ $-$ 4d$_+$ (J=2 to J=3) transition at 3483.2 mÅ has previously been observed in Alcator C-Mod plasmas [9]. Similar to the magnesiumlike transitions, the oxygenlike lines are observed at systematically longer wavelength than the predicted lines.

This is due to the configuration interaction between the J=0 levels in the ground and other J=0 levels up to and into the continuum.

V. HIGH-N TRANSITIONS AND CONFIGURATION INTERACTION EFFECTS

Higher n transitions have been observed for neonlike krypton, similar to those seen in Mo^{32+} [8,9]. Shown in Fig.10 are the 4D ($2p_+ - 4d_+$) and 4C ($2p_- - 4d_-$) lines of Kr^{26+} at 5396.4 and 5278.7 mÅ, respectively, along with neighboring satellites and the neonlike 4F ($2p_- - 4s_+$) line at 5407.3 mÅ. Central parameters for the plasma from which this spectrum was obtained were T_e = 1150 eV and $n_e = 1.6\times10^{14}/cm^3$. These transitions have been studied extensively in molybdenum [8,22]. Also shown in Fig.10 is a synthetic spectrum, which is in good agreement with the observations, although there is a ~ -10 mÅ shift of the calculated wavelength for the magnesiumlike $2p_- - 4d_-$ transition at 5436.6 mÅ. The 4F transition at 5407.3 mÅ is readily noticeable, having about 10% of the intensity of the 4D transition; the 4F line in Mo^{32+} at 3705.6 mÅ was too weak to be reported in Ref. [8], but has been observed here, with about 1% of the intensity of 4D. The reason the 4F line is so intense in Kr^{26+} is because of its close proximity to the 4D line; the upper levels are separated by only 4.6 eV, and significant configuration interaction results that transfers strength from 4D to 4F. This phenomenon has been seen between the 7D and 6C levels in Mo^{32+} [8,9,45], but in contrast here, the *longer* wavelength line is the beneficiary of the enhanced intensity. The energy level diagrams for n = 4 and 5 transitions in neonlike molybdenum and krypton are shown in Fig.11. As can be seen, the upper levels for the 4D and 4F transitions in Kr^{26+} are very close, while in Mo^{32+} these levels are 31 eV apart, too far away for any significant configuration interaction. The calculated oscillator strengths of the $2p_- - ns_+$ (nF) transitions as a function of n for Mo^{32+}, Nb^{31+}, Zr^{30+} and Kr^{26+} are shown in the top of Fig.12. Only in the case of Kr^{26+} are the 4D and 4F upper levels close enough to interact; as such the intensity of the 4F transition is enhanced by a factor of $\sim$50. The calculated and measured brightness ratios between the 4F and 4D transitions

are shown in Fig.13, as a function of the level separation of the upper levels for neonlike ions of the elements Br through Mo. The value of this ratio for Y^{29+} is suppressed by three orders of magnitude and does not appear on the plot. The agreement between theory and experiment is good and observations of the 4F/4D ratio in Rb^{27+} are planned; in the case of molybdenum, the 4F line is very weak, less than 1% of the intensity of the bright 4D line, but in good agreement with the calculations.

The Kr^{26+} $2p - nd$ series with n between 5 and 9 is shown in Fig.14; this is another composite spectrum taken during a series of similar discharges, with n_e = 1.8-2.8$\times 10^{14}$/cm^3 and T_e = 1200-1700 eV. Also visible in this spectrum are the Kr^{26+} 4A, 4B, 5A and 5B transitions and two strong Kr^{27+} lines, $2p_- - 4d_-$ at 5055.2 mÅ, and $2p_+ - 5d_+$ at 4701.0 mÅ. High n krypton lines are summarized in Table VIII. Similar high n transitions have been seen in molybdenum, niobium and zirconium [9,45]. Apparent from Figs.1, 9 and 14 and the Tables is that the $2s - np$ series is comprised of pairs of transitions, nA and nB, that have an intensity ratio of about 2.5 and upper levels which become closer together as n increases. The measured and calculated energy separation of these pairs of levels as a function of n is shown in Fig.15 for Mo^{32+} and Kr^{26+}. The agreement for the level separation is quite good, although the calculated wavelengths for these lines are significantly shifted from the measured values [8,9], for the reasons mentioned above. The measured transition pairs for n$\geq$7 [9] are actually too close together to resolve. (In Table II of Ref. [9] the calculated pairs of wavelengths for n=7, 8 and 9 should be switched.) The intensities of the $2s - np$ series transitions decrease strongly with increasing n. Shown in Fig.16 are the calculated oscillator strengths of the $2s - np$ transitions in neonlike molybdenum, niobium and krypton. The oscillator strengths decrease roughly as $1/n^3$, maintaining a ratio of about 2.5 for the two series. The 4B transition in Kr^{26+} (at 4968.2 mÅ) does not follow this trend and is about a factor of four lower. The reason for this can be seen in the energy level diagram, Fig.11: the upper level for 4B in krypton is within 2.2 eV of the upper level for 5G, there is significant configuration interaction and the intensity of 5G increases at the expense of 4B. For molybdenum, the upper level of 5G is 11.0 eV away from the upper level

of 4A and 23.4 eV away from the upper level of 4B, on the short wavelength side of both, and there is very little interaction.

These predicted configuration interaction effects are borne out by the observations, as can by seen in Fig.17, where the spectra in the vicinity of the 4A and 4B transitions in molybdenum and krypton are shown. Central plasma parameters for the molybdenum spectrum were $n_e = 1.6\times10^{14}/cm^3$ and $T_e = 1850$ eV, and for the krypton spectrum were $n_e = 1.8\times10^{14}/cm^3$ and $T_e = 1250$ eV. Also shown are the synthetic spectra, which are in good agreement with regard to line intensities, although the 4A and 4B lines are at significantly longer wavelengths than the predictions. In spite of the presence of three sodiumlike lines between the Mo^{32+} 4A and 4B lines, their ratio is close to what is expected from Fig.16. Their separation also agrees well with the predictions of Fig.15. The weak 5G transition at 3428.7 mÅ is also visible. For the case of krypton, shown in the bottom of Fig.17, the situation is different: the 4B transition at 4968.2 mÅ is relatively weak. The identification of this feature is based on the separation from the 4A transition at 4958.5 mÅ, and from the trends in Fig.15. The 5G line at 4972.6 mÅ is relatively bright due to configuration interaction with the upper level of 4B. This enhanced intensity for 5G is apparent from the bottom of Fig.12, as manifested by the enhanced oscillator strength, and is reflected in the synthetic spectrum of Fig.17. This selective configuration interaction effect in the Kr^{26+} 4B upper level is emphasized in Fig.18, where the brightness ratios of nA/nB are shown as a function of n for molybdenum and krypton, with excellent agreement between theory and experiment. In general the ratios are between 2.5 and 3, with the exception of Kr^{26+} 4A/4B, due to the configuration interaction effect described above. Spectra including 5A and 5B in molybdenum and krypton are shown in Fig.19. Central plasma parameters for the molybdenum spectrum were $n_e = 3.4\times10^{14}/cm^3$ and $T_e = 1900$ eV, and for the krypton spectrum were $n_e = 2.5\times10^{14}/cm^3$ and $T_e = 1750$ eV.

Yet another manifestation of the configuration interaction, this time in Mo^{32+}, is also demonstrated in Fig.19. The interacting states in this case are the upper levels for 7D and 6C. As was shown previously [8,9], the 6C transition in Mo^{32+} is suppressed relative to

7D. This is not the case for Kr^{26+} where the upper levels are 20 eV apart, as can be seen in the bottom of Fig.19. Nearby satellites in both the molybdenum and krypton spectra contaminate the 6C lines, but the effect is clear. The brightness ratios for these lines as a function of level separation are shown in Fig.20, which is similar to Fig.5 of Ref. [45], but with the inclusion of the krypton points. The agreement between experiment and theory is quite good; it would certainly be gratifying to verify that this effect changes sign in Tc or in Ru. It is noteworthy that in the case of the 2p − nd configuration interaction, as in Figs.19 and 20, the 'beneficiary' of the enhanced intensity is on the short wavelength side (higher energy side) whereas in the case of 2p − ns level enhancement, the 'beneficiaries' are on the long wavelength side (lower energy side) of the 'donor' transition.

Finally, it is interesting to note that there is no configuration interaction between the upper levels of E23 and 3F, even though these levels are only 2.3 eV apart in Kr^{26+}, as can be seen in Fig.7. This is because the upper levels are of opposite parity and cannot interact. Shown in Fig.21 are the calculated intensity ratios for E22/3F and E23/3F as a function of upper level energy separation in Kr, Zr, Nb and Mo; also shown are the measured ratios for Kr and Mo, in excellent agreement with theory. In contrast to the cases of Figs.13 and 20, here there is no resonant behavior within a few eV of zero energy separation for these transitions.

VI. CONCLUSIONS

2 − 3 transitions in neonlike Kr, Mo, Nb and Zr have been observed from Alcator C and Alcator C-Mod plasmas, in addition to associated fluorine-, sodium- and magnesiumlike satellites. Accurate wavelengths have been determined in reference to nearby calibration lines from hydrogen- and heliumlike ions. Measured wavelengths and line intensities have been compared with atomic structure calculations and collisional radiative modeling from the RELAC code, with very good overall agreement. A Z-scaling of the wavelengths of the brightest Na- and Mg-like satellites also shows good agreement with theory. Electric

and magnetic quadrupole transitions are found to be relatively intense (compared to bright allowed transitions in neonlike ions) for tokamak plasma conditions, again in good accord with the modeling. High n transitions (up to n=9) in neonlike krypton and molybdenum have also been recorded. Configuration interaction effects in certain line intensities have been observed, for transitions with nearly degenerate upper levels; comparison of observed line intensities with theory is excellent.

VII. ACKNOWLEDGEMENT

The authors would like to thank J. Irby for electron density measurements, A. Hubbard for electron temperature measurements and the Alcator operations groups for expert running of the tokamaks. Work supported at MIT by DoE Co-operative Agreement No. DE-FC02-99ER54512. This work was performed under the auspices of the U.S. Department of Energy by the University of California Lawrence Livermore National Laboratory under contract No. W-7405-Eng-48.

REFERENCES

[1] Burkhalter et al., Phys. Rev. A **18**, 718 (1978).

[2] H. Gordon, M.G. Hobby, N.J. Peacock and R.D. Cowan, J. Phys. B **12**, 881 (1979).

[3] Burkhalter et al., J. Appl. Phys. **50**, 4532 (1979).

[4] E.V. Aglitskii et al., Physica Scripta **40**, 601 (1989).

[5] E. Källne, J. Källne and R.D. Cowan, Phys. Rev. A **27**, 2682 (1983).

[6] P. Beiersdorfer et al., Phys. Rev. A **34**, 1297 (1986).

[7] P. Beiersdorfer et al., Phys. Rev. A **37**, 4153 (1988).

[8] J.E. Rice et al., Phys Rev A **51**, 3551 (1995).

[9] J.E. Rice et al., Phys. Rev. A **53**, 3953 (1996).

[10] D. Pacella et al., Phys. Rev. E **61**, 5701 (2000).

[11] S. Ya. Khakhalin et al., Phys. Scripta **50**, 106 (1994).

[12] S. Ya. Khakhalin et al., JETP **78**, 633 (1994).

[13] S. Ya. Khakhalin et al., J. Opt. Soc. Am. B **12**, 1203 (1995).

[14] M.D. Rosen et al., Phys. Rev. Lett., **54**, 106 (1985).

[15] D.L. Matthews et al., Phys. Rev. Lett., **54**, 110 (1985).

[16] A.L. Osterheld et al., J. Quant. Spectrosc. Radiat. Transfer, **51**, No. 1/2, 263 (1994).

[17] P. Beiersdorfer, M.H. Chen, R.E. Marrs and M. Levine, Phys. Rev. A **41**, 3453 (1990).

[18] G.A. Chandler, M.H. Chen, D.D. Dietrich, P.O. Egan, K.P. Ziock, P.H. Mokler, S. Reusch and D.H.H. Hoffmann, Phys. Rev. A, **39**, 565 (1989).

[19] D.D. Dietrich, G.A. Chandler, P.O. Egan, K.P. Ziock, P.H. Mokler, S. Reusch and

D.H.H. Hoffmann, Nucl. Instrum. Methods B, **24/25**, 301 (1987).

[20] E. Avgoustoglou, W.R. Johnson, Z.W. Liu and J. Sapirstein, Phys. Rev. A **51**, 1196 (1995).

[21] W.R. Johnson, J. Sapirstein and K.T. Cheng, Phys. Rev. A **51**, 297 (1995).

[22] J.E. Rice et al., J. Phys. B: At. Mol. Phys. **29**, 2191 (1996).

[23] K.B. Fournier et al., Phys. Rev. A **54**, 3870 (1996).

[24] K.B. Fournier, D. Pacella, M.J. May, M. Finkenthal and W.H. Goldstein, Nucl. Fusion **37**, 825 (1997). (corrigendum Nucl. Fusion **38**, 639 (1998).)

[25] G.V. Brown et al., Ap. J. **502**, 1015 (1998).

[26] M.Klapisch, Comput. Phys. Commun. **2**, 269 (1971).

[27] M.Klapisch, J.L.Schwob, B.S.Fraenkel and J.Oreg, J. Opt. Soc. Am. **67**, 148 (1977).

[28] P.J. Mohr, Phys. Rev. A, **26**, 2338 (1982) and references 1, 2 and 3 therein.

[29] R.R. Parker et al., Nucl. Fusion **25**, 1127 (1985).

[30] I.H.Hutchinson et al., Phys. Plasmas **1**, 1511 (1994).

[31] M.A.Graf et al., Rev. Sci. Instrum. **66**, 636 (1995).

[32] J.E.Rice and E.S.Marmar, Rev. Sci. Instrum. **61**, 2753 (1990).

[33] G.W.Erickson, J. Phys. Chem. Ref. Data **6**, 831 (1977).

[34] E.S.Marmar et al., Phys. Rev. A **33**, 774 (1986)

[35] J.F.Seely and U.Feldman, Phys. Rev. Lett. **54**, 1016 (1985).

[36] L.A.Vainshtein and U.I.Safronova, Physica Scripta **31**, 519 (1985).

[37] J.E. Rice et al., New J. Phys. **1**, 19 (1999).

[38] L.W. Fullerton and G.A. Rinker, Phys. Rev. A, **13**, 1283 (1976).

[39] I. P. Grant, J. Phys. B: At. Mol. Phys. **7**, 1458 (1974).

[40] J. Oreg, W. H. Goldstein, M. Klapisch, and A. Bar-Shalom, Phys. Rev. A **44**, 1750 (1991).

[41] A. Bar-Shalom, M. Klapisch, and J. Oreg, Phys. Rev. A **38**, 1773 (1988).

[42] R. D. Cowan, J. Physique Coll. C4 **31**, 191-201 (1970).

[43] M. Aymar, Nucl. Instrum. Methods **110**, 211-217 (1973).

[44] J. H. Parkinson, Astron. & Astrophys. **24**, 215 (1973).

[45] J. E. Rice, K. B. Fournier, J. L. Terry, M. Finkenthal, E. S. Marmar, W. H. Goldstein and U.I.Safronova, '2l - nl′ X-ray Transitions from Neonlike Charge States of the Row 5 Metals with $39 \leq Z \leq 46$', Proceedings of the 10th Topical Conference on Atomic Processes in Plasmas, San Francisco, CA, January 1996, AIP Press Conference Proceedings 381, Woodbury, NY, pp.11-20 (1996).

TABLES

TABLE I. $2-3$ transitions in neonlike Kr^{26+}. In the first and second columns are the measured and calculated wavelengths, in the third column are the transition labels, in the fourth column are the calculated oscillator strengths and in the last column are the transition designations (j-j coupling).

$\lambda_{\rm E}$	$\lambda_{\rm Th}$	Label	gf	Transition
6103.8	6093.2	E2s	–	$2s^2 2p^6$ J=0 – $2s 2p^6 3d_+$ J=2
	6123.4	(E2s)	–	$2s^2 2p^6$ J=0 – $2s 2p^6 3d_-$ J=2
6335.5	6324.0	3A	3.052[−1]	$2s^2 2p^6$ J=0 – $2s 2p^6 3p_+$ J=1
6385.2	6373.4	3B	8.747[−2]	$2s^2 2p^6$ J=0 – $2s 2p^6 3p_-$ J=1
6697.3	6691.9	3C	1.941[+0]	$2s^2 2p^6$ J=0 – $2s^2 2p_-^1 2p_+^4 3d_-$ J=1
6878.7	6874.4	3D	1.538[+0]	$2s^2 2p^6$ J=0 – $2s^2 2p_-^2 2p_+^3 3d_+$ J=1
6959.4	6958.7	3E	7.794[−3]	$2s^2 2p^6$ J=0 – $2s^2 2p_-^2 2p_+^3 3d_-$ J=1
6995.2	6992.9	E21	–	$2s^2 2p^6$ J=0 – $2s^2 2p_-^1 2p_+^4 3p_+$ J=2
7208.1	7206.5	E22	–	$2s^2 2p^6$ J=0 – $2s^2 2p_-^2 2p_+^3 3p_+$ J=2
7267.5	7265.9	3F	8.584[−2]	$2s^2 2p^6$ J=0 – $2s^2 2p_-^1 2p_+^4 3s_+$ J=1
7277.5	7275.0	E23	–	$2s^2 2p^6$ J=0 – $2s^2 2p_-^2 2p_+^3 3p_-$ J=2
7504.4	7501.7	3G	1.332[−1]	$2s^2 2p^6$ J=0 – $2s^2 2p_-^2 2p_+^3 3s_+$ J=1
7519.2	7516.5	M2	–	$2s^2 2p^6$ J=0 – $2s^2 2p_-^2 2p_+^3 3s_+$ J=2

TABLE II. $2-3$ transitions in fluorinelike Kr^{27+}. In the first and second columns are the measured and calculated wavelengths, in the third column are the calculated oscillator strengths and in the last column are the transition designations (j-j coupling).

λ_E	λ_{Th}	gf	Transition
5960.7	5949.5	5.317[−2]	$2s^2 2p^5$ J=3/2 – $2s^1 2p_-^2 2p_+^3 3p_+$ J=5/2
5960.7	5950.1	E2	$2s^2 2p^5$ J=3/2 – $2s^1 2p_-^2 2p_+^3 3d_+$ J=5/2
5960.7	5950.6	E2	$2s^2 2p^5$ J=3/2 – $2s^1 2p_-^2 2p_+^3 3d_+$ J=7/2
6015.0	6008.7	E2	$2s^2 2p^5$ J=3/2 – $2s^1 2p_-^2 2p_+^3 3d_+$ J=7/2
6015.0	6012.9	E2	$2s^2 2p^5$ J=3/2 – $2s^1 2p_-^2 2p_+^3 3d_+$ J=5/2
6143.6	6139.1	2.677[−1]	$2s^2 2p^5$ J=3/2 – $2s^1 2p_-^2 2p_+^3 3p_+$ J=5/2
	6172.4	2.761[−1]	$2s^2 2p^5$ J=3/2 – $2s^1 2p_-^2 2p_+^3 3p_+$ J=1/2
	6178.8	2.401[−1]	$2s^2 2p^5$ J=3/2 – $2s^1 2p_-^2 2p_+^3 3p_-$ J=3/2
6206.1	6202.1	2.772[−1]	$2s^2 2p^5$ J=3/2 – $2s^1 2p_-^2 2p_+^3 3p_+$ J=5/2
6216.6	6211.6	1.877[−1]	$2s^2 2p^5$ J=3/2 – $2s^1 2p_-^2 2p_+^3 3p_+$ J=3/2
6259.4	6253.5	1.897[−1]	$2s^2 2p^5$ J=3/2 – $2s^1 2p_-^2 2p_+^3 3p_-$ J=5/2
6432.1	6431.7	4.571[−1]	$2s^2 2p^5$ J=3/2 – $2s^2 2p_-^1 2p_+^3 3d_+$ J=3/2
6466.0	6461.3	2.832[+0]	$2s^2 2p^5$ J=3/2 – $2s^2 2p_-^1 2p_+^3 3d_-$ J=5/2
6466.0	6466.5	1.857[+0]	$2s^2 2p^5$ J=3/2 – $2s^2 2p_-^1 2p_+^3 3d_-$ J=3/2
6479.0	6476.8	1.122[−1]	$2s^2 2p^5$ J=3/2 – $2s^2 2p_-^1 2p_+^3 3d_+$ J=5/2
6479.0	6477.4	8.548[−1]	$2s^2 2p^5$ J=3/2 – $2s^2 2p_-^1 2p_+^3 3d_-$ J=1/2
	6514.6	4.575[−1]	$2s^2 2p^5$ J=3/2 – $2s^2 2p_-^1 2p_+^3 3d_+$ J=5/2
6519.4	6520.5	6.455[−1]	$2s^2 2p^5$ J=3/2 – $2s^2 2p_-^1 2p_+^3 3d_-$ J=5/2
6531.9	6538.7	4.547[−2]	$2s^2 2p^5$ J=3/2 – $2s^2 2p_-^1 2p_+^3 3d_-$ J=3/2
6593.9	6593.6	2.300[−2]	$2s^1 2p^6$ J=1/2 – $2s^1 2p_-^1 2p_+^4 3d_-$ J=3/2
6608.5	6611.2	1.512[+0]	$2s^2 2p^5$ J=1/2 – $2s^2 2p_-^1 2p_+^3 3d_+$ J=1/2
6615.6	6621.7	2.041[+0]	$2s^2 2p^5$ J=1/2 – $2s^2 2p_-^1 2p_+^3 3d_+$ J=3/2
6626.5	6622.4	1.033[+0]	$2s^2 2p^5$ J=3/2 – $2s^2 2p_-^2 2p_+^2 3d_+$ J=5/2

6638.9	6635.3	5.402[−1]	$2s^2 2p^5$ J=3/2 – $2s^2 2p_-^2 2p_+^2 3d_-$ J=3/2
	6658.6	3.220[−1]	$2s^2 2p^5$ J=1/2 – $2s^2 2p_-^1 2p_+^3 3d_-$ J=3/2
6662.7	6661.7	1.659[+0]	$2s^2 2p^5$ J=3/2 – $2s^2 2p_-^2 2p_+^2 3d_+$ J=5/2
	6670.1	7.510[−2]	$2s^2 2p^5$ J=1/2 – $2s^2 2p_-^1 2p_+^3 3d_-$ J=1/2
6675.4	6675.0	8.210[−1]	$2s^2 2p^5$ J=3/2 – $2s^2 2p_-^2 2p_+^2 3d_+$ J=3/2
6725.9	6721.7	8.379[−2]	$2s^1 2p^6$ J=1/2 – $2s^1 2p_-^2 2p_+^3 3d_-$ J=3/2
6725.9	6723.5	2.696[−1]	$2s^1 2p^6$ J=1/2 – $2s^1 2p_-^2 2p_+^3 3d_-$ J=1/2
	6777.5	3.361[−1]	$2s^1 2p^6$ J=1/2 – $2s^1 2p_-^2 2p_+^3 3d_+$ J=3/2
	6891.7	E2	$2s^2 2p^5$ J=3/2 – $2s^2 2p_-^2 2p_+^2 3p_+$ J=3/2
6897.2	6899.9	E2	$2s^2 2p^5$ J=1/2 – $2s^2 2p_-^1 2p_+^3 3p_+$ J=5/2
	6903.1	E2	$2s^2 2p^5$ J=1/2 – $2s^2 2p_-^1 2p_+^3 3p_-$ J=3/2
6937.0	6939.5	5.204[−3]	$2s^2 2p^5$ J=1/2 – $2s^2 2p_-^2 2p_+^2 3d_-$ J=3/2
6944.4	6945.6	1.860[−1]	$2s^2 2p^5$ J=3/2 – $2s^2 2p_-^1 2p_+^3 3s_+$ J=5/2
	6954.1	E2	$2s^2 2p^5$ J=3/2 – $2s^2 2p_-^2 2p_+^2 3p_+$ J=7/2
	6957.7	E2	$2s^2 2p^5$ J=3/2 – $2s^2 2p_-^2 2p_+^2 3p_+$ J=5/2
	6957.7	E2	$2s^2 2p^5$ J=1/2 – $2s^2 2p_-^1 2p_+^3 3p_-$ J=5/2
6990.0	7000.5	6.299[−2]	$2s^2 2p^5$ J=3/2 – $2s^2 2p_-^1 2p_+^3 3s_+$ J=3/2
7007.0	7007.2	E2	$2s^2 2p^5$ J=3/2 – $2s^2 2p_-^2 2p_+^2 3p_-$ J=5/2
7121.8	7119.9	5.439[−2]	$2s^2 2p^5$ J=3/2 – $2s^2 2p_-^2 2p_+^2 3s_+$ J=1/2
7160.0	7160.9	1.733[−1]	$2s^2 2p^5$ J=1/2 – $2s^2 2p_-^1 2p_+^3 3s_+$ J=3/2
7192.3	7193.1	2.551[−1]	$2s^2 2p^5$ J=3/2 – $2s^2 2p_-^2 2p_+^2 3s_+$ J=3/2
7200.1	7201.5	2.334[−2]	$2s^1 2p^6$ J=1/2 – $2s^1 2p_-^2 2p_+^3 3s_+$ J=3/2
7211.7	7214.5	4.213[−2]	$2s^2 2p^5$ J=3/2 – $2s^2 2p_-^2 2p_+^2 3s_+$ J=5/2

TABLE III. $2-3$ transitions in sodiumlike Kr^{25+}. The legend is the same as in Table II.

λ_E	λ_{Th}	gf	Transition
	6336.8	8.17[−2]	$2s^2 2p^6 3s$ J=1/2 – $2s^1 2p^6 3s_+ 3p_+$ J=1/2
6398.2	6386.3	4.20[−1]	$2s^2 2p^6 3s$ J=1/2 – $2s^1 2p^6 3s_+ 3p_+$ J=3/2
6419.4	6414.6	1.57[−1]	$2s^2 2p^6 3s$ J=1/2 – $2s^1 2p^6 3s_+ 3p_-$ J=1/2
6714.5	6708.4	1.00[+0]	$2s^2 2p^6 3s$ J=1/2 – $2s^2 2p_-^1 2p_+^4 3s_+ 3d_+$ J=3/2
6755.6	6752.6	9.10[−1]	$2s^2 2p^6 3s$ J=1/2 – $2s^2 2p_-^1 2p_+^4 3s_+ 3d_-$ J=1/2 [a]
6755.6	6755.6	1.76[+0]	$2s^2 2p^6 3p_+$ J=3/2 – $2s^2 2p_-^1 2p_+^4 3p_+ 3d_-$ J=3/2
6755.6	6759.3	4.01[−1]	$2s^2 2p^6 3s$ J=1/2 – $2s^2 2p_-^1 2p_+^4 3p_+^2$ J=1/2
6768.8	6769.0	1.41[+0]	$2s^2 2p^6 3s$ J=1/2 – $2s^2 2p_-^1 2p_+^4 3s_+ 3d_-$ J=3/2
6776.4	6770.0	6.50[−2]	$2s^2 2p^6 3p_-$ J=1/2 – $2s^2 2p_-^1 2p_+^4 3p_- 3d_-$ J=3/2
6847.2	6830.7	6.31[−2]	$2s^2 2p^6 3s$ J=1/2 – $2s^2 2p_-^1 2p_+^4 3p_+^2$ J=3/2 [a]
6886.3	6874.6	6.82[−2]	$2s^2 2p^6 3s$ J=1/2 – $2s^2 2p_-^1 2p_+^4 3p_- 3p_+$ J=3/2 [a]
6912.6	6908.3	9.84[−1]	$2s^2 2p^6 3s$ J=1/2 – $2s^2 2p_-^2 2p_+^3 3s_+ 3d_+$ J=3/2
6921.1	6919.2	6.51[−1]	$2s^2 2p^6 3s$ J=1/2 – $2s^2 2p_-^2 2p_+^3 3s_+ 3d_+$ J=1/2
6953.7	6953.1	5.34[−1]	$2s^2 2p^6 3s$ J=1/2 – $2s^2 2p_-^2 2p_+^3 3s_+ 3d_+$ J=3/2
6975.4	6974.3	2.75[−1]	$2s^2 2p^6 3s$ J=1/2 – $2s^2 2p_-^2 2p_+^3 3s_+ 3d_-$ J=1/2
7303.3	7305.4	2.71[−2]	$2s^2 2p^6 3d_+$ J=5/2 – $2s^2 2p_-^1 2p_+^4 3s_+ 3d_+$ J=5/2
7321.1	7320.0	4.90[−2]	$2s^2 2p^6 3p_-$ J=1/2 – $2s^2 2p_-^1 2p_+^4 3s_+ 3p_-$ J=1/2
7349.0	7349.4	1.88[−2]	$2s^2 2p^6 3d_-$ J=3/2 – $2s^2 2p_-^1 2p_+^4 3s_+ 3d_-$ J=3/2
	7360.5	3.23[−2]	$2s^2 2p^6 3d_+$ J=5/2 – $2s^2 2p_-^1 2p_+^4 3s_+ 3d_-$ J=3/2
	7377.0	7.20[−1]	$2s^2 2p^6 3p_+$ J=3/2 – $2s^2 2p_-^1 2p_+^4 3s_+ 3p_+$ J=1/2
7376.2	7376.1	6.45[−2]	$2s^2 2p^6 3p_+$ J=3/2 – $2s^2 2p_-^1 2p_+^4 3s_+ 3p_-$ J=1/2
7384.1	7381.6	3.70[−2]	$2s^2 2p^6 3d_-$ J=3/2 – $2s^2 2p_-^1 2p_+^4 3s_+ 3d_+$ J=5/2
7393.6	7393.6	7.76[−2]	$2s^2 2p^6 3p_-$ J=1/2 – $2s^2 2p_-^1 2p_+^4 3s_+ 3p_-$ J=3/2
	7394.3	8.10[−2]	$2s^2 2p^6 3p_-$ J=1/2 – $2s^2 2p_-^1 2p_+^4 3s_+ 3p_-$ J=3/2
7402.3	7400.3	1.43[−1]	$2s^2 2p^6 3p_+$ J=3/2 – $2s^2 2p_-^1 2p_+^4 3s_+ 3p_+$ J=5/2

	7518.2	4.80[−2]	$2s^2 2p^6 3d_-$ J=3/2 – $2s^2 2p_-^2 2p_+^3 3s_+ 3d_+$ J=5/2
	7538.5	3.22[−2]	$2s^2 2p^6 3d_+$ J=5/2 – $2s^2 2p_-^2 2p_+^3 3s_+ 3d_+$ J=5/2
	7557.0	6.46[−2]	$2s^2 2p^6 3d_+$ J=5/2 – $2s^2 2p_-^2 2p_+^3 3s_+ 3d_+$ J=7/2
	7559.8	7.03[−2]	$2s^2 2p^6 3p_+$ J=3/2 – $2s^2 2p_-^2 2p_+^3 3s_+ 3p_+$ J=3/2
7574.1	7572.4	1.00[−1]	$2s^2 2p^6 3p_+$ J=3/2 – $2s^2 2p_-^2 2p_+^3 3s_+ 3p_+$ J=5/2
7582.9	7587.1	4.18[−2]	$2s^2 2p^6 3d_+$ J=5/2 – $2s^2 2p_-^2 2p_+^3 3s_+ 3d_+$ J=3/2
7601.9	7601.9	1.29[−1]	$2s^2 2p^6 3s$ J=1/2 – $2s^2 2p_-^2 2p_+^3 3s^2$ J=3/2

[a] enabled by mixing between $2s^2 2p^5 3s 3d$ + $2s^2 2p^5 3p^2$

TABLE IV. $2-3$ transitions in magnesiumlike Kr^{24+}. The legend is the same as in Table II.

λ_E	λ_{Th}	gf	Transition
	6430.3	2.93[−1]	$2s^2 2p^6 3s^2$ J=0 – $2s^1 2p^6 3s^2 3p_+$ J=1
6790.9	6789.2	1.86[+0]	$2s^2 2p^6 3s^2$ J=0 – $2s^2 2p_-^1 2p_+^4 3s^2 3d_-$ J=1
	6918.7	2.40[−1]	$2s^2 2p^6 3s^2$ J=0 – $2s^2 2p_-^1 2p_+^4 3s_+ 3p_- 3p_+$ J=1 [a]
6979.0	6976.6	1.57[+0]	$2s^2 2p^6 3s^2$ J=0 – $2s^2 2p_-^2 2p_+^3 3s^2 3d_+$ J=1
	6987.0	1.50[−1]	$2s^2 2p^6 3s^2$ J=0 – $2s^2 2p_-^1 2p_+^4 3s_+ 3p_-^2$ J=1 [a]
	7013.0	1.90[−1]	$2s^2 2p^6 3s^2$ J=0 – $2s^2 2p_-^2 2p_+^3 3s_+ 3p_+^2$ J=1 [a]
7418.1	7421.9	6.44[−2]	$2s^2 2p^6 3s 3d_+$ J=3 – $2s^2 2p_-^1 2p_+^4 3s^2 3d_+$ J=3

[a] enabled by mixing between $2s^2 2p^5 3s^2 3d + 2s^2 2p^5 3s 3p^2$

TABLE V. $2-3$ transitions in neonlike Mo^{32+} and associated satellites. In the first and second columns are the measured and calculated wavelengths, in the third column is the iso-electronic sequence (with the neonlike transition label), in the fourth column are the calculated oscillator strengths and in the last column are the transition designations (j-j coupling).

λ_E	λ_{Th}	Ion (Label)	gf	Transition
4276.2	4270.9	Ne (E2s)	–	$2s^2 2p^6$ J=0 – $2s 2p^6 3d_+$ J=2
4343.2	4341.0	F	2.857[−1]	$2s^2 2p^5$ J=3/2 – $2s^1_+ 2p^2_- 2p^3_+ 3p_+$ J=5/2
4370.5	4368.4	O	1.290[+0]	$2s^2 2p^2_- 2p^2_+$ J=2 – $2s^2 2p^1_- 2p^2_+ 3d_-$ J=2
4370.5	4368.7	O	8.384[−1]	$2s^2 2p^2_- 2p^2_+$ J=2 – $2s^2 2p^1_- 2p^2_+ 3d_-$ J=1
4370.5	4370.6	O	1.336[+0]	$2s^2 2p^2_- 2p^2_+$ J=0 – $2s^2 2p^1_- 2p^2_+ 3d_-$ J=1
4377.7	4376.9	O	3.031[+0]	$2s^2 2p^2_- 2p^2_+$ J=2 – $2s^2 2p^1_- 2p^2_+ 3d_-$ J=3
4379.4	4383.1	O	8.742[−1]	$2s^2 2p^2_- 2p^2_+$ J=2 – $2s^2 2p^1_- 2p^2_+ 3d_+$ J=2
4408.2	4408.7	O	4.775[−1]	$2s^2 2p^2_- 2p^2_+$ J=2 – $2s^2 2p^1_- 2p^2_+ 3d_-$ J=3
4417.6	4413.1	Ne (3A)	3.120[−1]	$2s^2 2p^6$ J=0 – $2s 2p^6 3p_+$ J=1
4420.9	4416.9	O	8.198[−2]	$2s^2 2p^2_- 2p^2_+$ J=2 – $2s^2 2p^1_- 2p^2_+ 3d_-$ J=1
4423.8	4422.5	Na	1.151[−1]	$2s^2 2p^6 3s$ J=1/2 – $2s 2p^6 3s 3p_+$ J=1/2
4444.5	4449.1	Na	4.370[−1]	$2s^2 2p^6 3s$ J=1/2 – $2s 2p^6 3s 3p_+$ J=3/2
4464.8	4460.1	Ne (3B)	1.077[−1]	$2s^2 2p^6$ J=0 – $2s 2p^6 3p_-$ J=1
4498.3	4496.4	F	2.325[+0]	$2s^2 2p^5$ J=3/2 – $2s^2 2p^1_- 2p^3_+ 3d_-$ J=5/2
4498.3	4498.4	F	1.751[+0]	$2s^2 2p^5$ J=3/2 – $2s^2 2p^1_- 2p^3_+ 3d_-$ J=3/2
4504.5	4504.4	F	8.393[−1]	$2s^2 2p^5$ J=3/2 – $2s^2 2p^1_- 2p^3_+ 3d_-$ J=1/2
4528.4	4529.3	F	8.313[−1]	$2s^2 2p^5$ J=3/2 – $2s^2 2p^1_- 2p^3_+ 3d_-$ J=5/2
4535.8	4533.3	O	3.288[+0]	$2s^2 2p^2_- 2p^2_+$ J=2 – $2s^2 2p^2_- 2p^1_+ 3d_+$ J=3
4535.8	4537.6	O	8.972[−1]	$2s^2 2p^1_- 2p^3_+$ J=1 – $2s^2 2p^1_- 2p^2_+ 3d_-$ J=2
4553.2	4551.4	O	1.073[+0]	$2s^2 2p^2_- 2p^2_+$ J=2 – $2s^2 2p^2_- 2p^1_+ 3d_+$ J=2
4572.8	4573.5	O	9.523[−1]	$2s^2 2p^2_- 2p^2_+$ J=0 – $2s^2 2p^2_- 2p^1_+ 3d_+$ J=1
4630.6	4628.5	Ne (3C)	1.672[+0]	$2s^2 2p^6$ J=0 – $2s^2 2p^1_- 2p^4_+ 3d_-$ J=1

4635.5	4632.6	Na	7.785[−1]	$2s^2 2p^6 3s$ J=1/2 – $2s^2 2p^1_- 2p^4_+ 3s 3d_+$ J=3/2
4648.4	4646.7	Na	1.538[+0]	$2s^2 2p^6 3p$ J=3/2 – $2s^2 2p^1_- 2p^4_+ 3p_+ 3d_-$ J=5/2
4654.6	4652.9	F	1.586[+0]	$2s^2 2p^5$ J=3/2 – $2s^2 2p^2_- 2p^2_+ 3d_+$ J=5/2
4665.1	4664.2	Na	1.125[+0]	$2s^2 2p^6 3s$ J=1/2 – $2s^2 2p^1_- 2p^4_+ 3s 3d_-$ J=1/2
4665.1	4665.4	F	8.555[−1]	$2s^2 2p^5$ J=3/2 – $2s^2 2p^2_- 2p^2_+ 3d_-$ J=3/2
4670.1	4670.0	Na	1.322[+0]	$2s^2 2p^6 3s$ J=1/2 – $2s^2 2p^1_- 2p^4_+ 3s 3d_-$ J=3/2
4680.9	4679.1	F	1.867[+0]	$2s^2 2p^5$ J=3/2 – $2s^2 2p^2_- 2p^2_+ 3d_+$ J=5/2
4682.5	4683.9	Mg	1.646[+0]	$2s^2 2p^6 3s^2$ J=0 – $2s^2 2p^1_- 2p^4_+ 3s^2 3d_-$ J=1
	4688.5	F	8.194[−1]	$2s^2 2p^5$ J=3/2 – $2s^2 2p^2_- 2p^2_+ 3d_+$ J=3/2
4800.4	4801.0	Ne (E21)	–	$2s^2 2p^6$ J=0 – $2s^2 2p^1_- 2p^4_+ 3p_+$ J=2
4804.5	4802.6	Ne (3D)	1.869[+0]	$2s^2 2p^6$ J=0 – $2s^2 2p^2_- 2p^3_+ 3d_+$ J=1
4809.7				
4815.5	4815.7	Na	7.480[−1]	$2s^2 2p^6 3s$ J=1/2 – $2s^2 2p^2_- 2p^3_+ 3p^2_+$ J=3/2 [a]
4817.9				
4826.3	4825.0	Na	8.544[−1]	$2s^2 2p^6 3s$ J=1/2 – $2s^2 2p^2_- 2p^3_+ 3s 3d_+$ J=1/2
	4836.0	Na	3.731[−1]	$2s^2 2p^6 3s$ J=1/2 – $2s^2 2p^2_- 2p^3_+ 3p^2_+$ J=3/2
4839.1	4839.8	O	1.207[−1]	$2s^2 2p^2_- 2p^2_+$ J=2 – $2s^2 2p^2_- 2p^1_+ 3s$ J=2
4847.2	4846.2	Na	1.351[+0]	$2s^2 2p^6 3s$ J=1/2 – $2s^2 2p^2_- 2p^3_+ 3s 3d_+$ J=3/2
4851.8	4852.3	Na	1.458[+0]	$2s^2 2p^6 3p$ J=3/2 – $2s^2 2p^2_- 2p^3_+ 3p_+ 3d_+$ J=5/2
4856.1	4859.3	Ne (3E)	2.391[−3]	$2s^2 2p^6$ J=0 – $2s^2 2p^2_- 2p^3_+ 3d_-$ J=1
4859.8	4860.2	F (E2)	–	$2s^2 2p^5$ J=3/2 – $2s^2 2p^2_- 2p^2_+ 3p_+$ J=7/2
4859.8	4862.0	F (E2)	–	$2s^2 2p^5$ J=3/2 – $2s^2 2p^2_- 2p^2_+ 3p_+$ J=5/2
4863.4	4864.1	Na	3.340[−1]	$2s^2 2p^6 3s$ J=1/2 – $2s^2 2p^2_- 2p^3_+ 3s 3d_-$ J=1/2
4870.8	4862.3	Mg	1.906[+0]	$2s^2 2p^6 3s^2$ J=0 – $2s^2 2p^2_- 2p^3_+ 3s^2 3d_+$ J=1
4881.5	4884.0	O	5.507[−2]	$2s 2p^2_- 2p^3_+$ J=1 – $2s 2p^2_- 2p^2_+ 3s$ J=2
4887.7	4890.3	O	2.386[−1]	$2s 2p^2_- 2p^3_+$ J=2 – $2s 2p^2_- 2p^2_+ 3s$ J=2
4982.9	4982.0	Ne (3F)	8.664[−2]	$2s^2 2p^6$ J=0 – $2s^2 2p^1_- 2p^4_+ 3s$ J=1

5008.4	5007.0	Ne (E22)	–	$2s^2 2p^6$ J=0 – $2s^2 2p_-^2 2p_+^3 3p_+$ J=2
	5011.1	Na	3.644[−2]	$2s^2 2p^6 3p$ J=1/2 – $2s^2 2p_-^1 2p_+^4 3s 3p_-$ J=1/2
5027.1	5027.1	F	2.483[−1]	$2s^2 2p^5$ J=3/2 – $2s^2 2p_-^2 2p_+^2 3s$ J=3/2
5029.2	5027.4	Mg	1.237[−2]	$2s^2 2p^6 3s 3p_-$ J=1 – $2s^2 2p_-^1 2p_+^4 3s^2 3p_-$ J=0
5039.0	5039.1	F	4.974[−2]	$2s^2 2p^5$ J=3/2 – $2s^2 2p_-^2 2p_+^2 3s$ J=5/2
5055.7	5057.9	Na	1.462[−1]	$2s^2 2p^6 3p$ J=3/2 – $2s^2 2p_-^1 2p_+^4 3s 3p_+$ J=5/2
5059.9	5058.7	O	6.350[−3]	$2s 2p_-^2 2p_+^3$ J=2 – $2s^2 2p_-^1 2p_+^2 3p_-$ J=2 [b]
5066.4	5065.9	Na	3.811[−2]	$2s^2 2p^6 3p$ J=3/2 – $2s^2 2p_-^1 2p_+^4 3s 3p_-$ J=1/2
5072.8	5070.6	Ne (E23)	–	$2s^2 2p^6$ J=0 – $2s^2 2p_-^2 2p_+^3 3p_-$ J=2
5206.0	5206.4	Ne (3G)	1.316[−1]	$2s^2 2p^6$ J=0 – $2s^2 2p_-^2 2p_+^3 3s$ J=1
5214.6	5215.0	Ne (M2)	–	$2s^2 2p^6$ J=0 – $2s^2 2p_-^2 2p_+^3 3s$ J=2
5228.0	5227.1	Na	3.407[−2]	$2s^2 2p^6 3d$ J=5/2 – $2s^2 2p_-^2 2p_+^3 3s 3d_+$ J=5/2
5238.8	5237.5	Na	6.056[−2]	$2s^2 2p^6 3d$ J=5/2 – $2s^2 2p_-^2 2p_+^3 3s 3d_+$ J=7/2
5246.9	5250.0	Na	1.092[−1]	$2s^2 2p^6 3p$ J=3/2 – $2s^2 2p_-^2 2p_+^3 3s 3p_+$ J=5/2
5259.7	5263.8	Na	1.260[−1]	$2s^2 2p^6 3s$ J=1/2 – $2s^2 2p_-^2 2p_+^3 3s^2$ J=3/2
5273.8	5275.8	Na	9.232[−2]	$2s^2 2p^6 3d$ J=5/2 – $2s^2 2p_-^2 2p_+^3 3s 3d_+$ J=7/2
5281.0	5279.1	Na	5.709[−2]	$2s^2 2p^6 3p$ J=3/2 – $2s^2 2p_-^2 2p_+^3 3s 3p_+$ J=1/2
5281.0	5279.4	Na	8.349[−2]	$2s^2 2p^6 3d$ J=3/2 – $2s^2 2p_-^2 2p_+^3 3s 3d_-$ J=5/2
5284.3	5285.4	Na	1.413[−1]	$2s^2 2p^6 3p$ J=1/2 – $2s^2 2p_-^2 2p_+^3 3s 3p_-$ J=3/2
5289.7	5289.1	Na	1.017[−1]	$2s^2 2p^6 3p$ J=3/2 – $2s^2 2p_-^2 2p_+^3 3s 3p_+$ J=5/2
5297.7	5304.2	Na (E2)	–	$2s^2 2p^6 3p$ J=3/2 – $2s^2 2p_-^2 2p_+^3 3s 3p_+$ J=7/2
5311.5	5317.6	F	3.403[−3]	$2s 2p^6$ J=1/2 – $2s^2 2p_-^1 2p_+^3 3p_-$ J=3/2 [c]
	5349.6	Na	1.216[−1]	$2s^2 2p^6 3p$ J=3/2 – $2s^2 2p_-^2 2p_+^3 3s 3p_-$ J=5/2

[a] enabled by mixing between $2p^5 3s^2 + 2p^5 3s 3d + 2p^5 3p^2$

[b] enabled by mixing between $2s 2p^4 3s + 2s 2p^4 3d + 2s^2 2p^3 3p$

[c] enabled by mixing between $2s 2p^5 3s + 2s 2p^5 3d + 2s^2 2p^4 3p$

TABLE VI. $2-3$ transitions in neonlike Nb^{31+} and associated satellites. The legend is the same as in Table V.

λ_E	λ_{Th}	Ion (Label)	gf	Transition
	4757.7	F	2.426[+0]	$2s^22p^5$ J=3/2 – $2s^22p_-^12p_+^33d_-$ J=5/2
	4760.1	F	1.761[+0]	$2s^22p^5$ J=3/2 – $2s^22p_-^12p_+^33d_-$ J=3/2
	4784.1	O	3.210[+0]	$2s^22p_-^22p_+^2$ J=2 – $2s^22p_+^22p_+^13d_+$ J=3
	4787.9	O	8.437[−1]	$2s^22p_-^12p_+^3$ J=1 – $2s^22p_+^12p_+^23d_-$ J=2
	4793.7	F	8.413[−1]	$2s^22p^5$ J=3/2 – $2s^22p_-^12p_+^33d_-$ J=5/2
	4803.9	O	1.039[+0]	$2s^22p_-^22p_+^2$ J=2 – $2s^22p_+^22p_+^13d_+$ J=2
	4805.1	O	7.840[−1]	$2s^22p_-^12p_+^3$ J=1 – $2s^22p_+^12p_+^23d_+$ J=2
	4828.7	O	9.430[−1]	$2s^22p_-^22p_+^2$ J=0 – $2s^22p_+^22p_+^13d_+$ J=1
	4902.9	O	2.236[−1]	$2s^22p_-^22p_+^2$ J=2 – $2s^22p_+^12p_+^23s$ J=3
4904.3	4901.8	Ne (3C)	1.704[+0]	$2s^22p^6$ J=0 – $2s^22p_-^12p_+^43d_-$ J=1
4909.8	4907.2	Na	8.201[−1]	$2s^22p^63s$ J=1/2 – $2s^22p_-^12p_+^43s3d_-$ J=3/2
4916.2	4914.3	F	1.518[+0]	$2s^22p^5$ J=3/2 – $2s^22p_-^22p_+^23d_+$ J=5/2
4923.8	4921.1	Na	1.536[+0]	$2s^22p^63p_+$ J=3/2 – $2s^22p_-^12p_+^43p_+3d_-$ J=5/2
4929.6	4927.0	F	7.996[−1]	$2s^22p^5$ J=3/2 – $2s^22p_-^22p_+^23d_-$ J=3/2
4941.5	4940.5	Na	1.147[+0]	$2s^22p^63s$ J=1/2 – $2s^22p_-^12p_+^43s3d_-$ J=1/2
4944.0	4942.4	F	1.844[+0]	$2s^22p^5$ J=3/2 – $2s^22p_-^22p_+^23d_+$ J=5/2
4947.7	4947.3	Na	1.323[+0]	$2s^22p^63s$ J=1/2 – $2s^22p_-^12p_+^43s3d_+$ J=3/2
4952.5	4952.3	F	8.357[−1]	$2s^22p^5$ J=3/2 – $2s^22p_-^22p_+^23d_+$ J=3/2
4962.0	4961.8	Mg	1.723[+0]	$2s^22p^63s^2$ J=0 – $2s^22p_-^12p_+^43s^23d_-$ J=1
4982.7	4983.4	F	2.459[−2]	$2s2p^6$ J=1/2 – $2s2p_-^22p_+^33d_-$ J=1/2
5077.8	5076.8	Ne (3D)	1.824[+0]	$2s^22p^6$ J=0 – $2s^22p_-^22p_+^33d_+$ J=1
5081.6	5083.8	F	1.914[−1]	$2s^22p^5$ J=3/2 – $2s^22p_-^12p_+^33s$ J=5/2
5089.1				
5094.6	5092.5	Na	8.432[−1]	$2s^22p^63s$ J=1/2 – $2s^22p_-^22p_+^33p_+^2$ J=3/2 [a]

	5098.9	O	1.541[−1]	$2s^2 2p_-^2 2p_+^2$ J=2 – $2s^2 2p_+^2 2p_+^1 3s$ J=1
5102.1	5101.2	Na	8.309[−1]	$2s^2 2p^6 3s$ J=1/2 – $2s^2 2p_-^2 2p_+^3 3s 3d_+$ J=1/2
5107.7	5106.6	F	4.544[−2]	$2s^2 2p^5$ J=3/2 – $2s^2 2p_-^1 2p_+^3 3s$ J=1/2
	5111.4	O	1.155[−1]	$2s^2 2p_-^2 2p_+^2$ J=2 – $2s^2 2p_+^2 2p_+^1 3s$ J=2
5117.6	5116.8	F	5.862[−2]	$2s^2 2p^5$ J=3/2 – $2s^2 2p_-^1 2p_+^3 3s$ J=3/2
5125.9	5125.2	Na	1.191[+0]	$2s^2 2p^6 3s$ J=1/2 – $2s^2 2p_-^2 2p_+^3 3s 3d_+$ J=3/2
5128.6	5129.9	Na	1.490[+0]	$2s^2 2p^6 3p_+$ J=3/2 – $2s^2 2p_-^2 2p_+^3 3s 3d_-$ J=5/2
5135.9	5141.2	Mg	1.918[+0]	$2s^2 2p^6 3s^2$ J=0 – $2s^2 2p_-^2 2p_+^3 3s^2 3d_+$ J=1
5142.2	5142.5	Na	3.250[−1]	$2s^2 2p^6 3s$ J=1/2 – $2s^2 2p_-^2 2p_+^3 3s 3d_-$ J=1/2
5150.8				
	5159.9	O	5.223[−2]	$2s 2p_-^2 2p_+^3$ J=1 – $2s 2p_-^2 2p_+^2 3s$ J=2
	5164.8	O	2.404[−1]	$2s 2p_-^2 2p_+^3$ J=2 – $2s 2p_-^2 2p_+^2 3s$ J=2
	5262.9	F	5.811[−2]	$2s^2 2p^5$ J=3/2 – $2s^2 2p_-^2 2p_+^2 3s$ J=1/2
5271.8				
5281.7	5282.2	Ne (3F)	8.564[−2]	$2s^2 2p^6$ J=0 – $2s^2 2p_-^1 2p_+^4 3s$ J=1
5297.8				
	5313.1	F	2.497[−1]	$2s^2 2p^5$ J=3/2 – $2s^2 2p_-^2 2p_+^2 3s$ J=3/2
	5314.0	Na	3.325[−2]	$2s^2 2p^6 3p$ J=1/2 – $2s^2 2p_-^1 2p_+^4 3s 3p_-$ J=1/2
5333.6	5326.2	F	4.880[−2]	$2s^2 2p^5$ J=3/2 – $2s^2 2p_-^2 2p_+^2 3s$ J=5/2
	5346.4	O	7.174[−3]	$2s 2p_-^2 2p_+^3$ J=2 – $2s^2 2p_-^1 2p_+^2 3p_-$ J=2 [b]
5362.6	5368.9	Na	4.198[−2]	$2s^2 2p^6 3p_+$ J=3/2 – $2s^2 2p_-^1 2p_+^4 3s 3p_-$ J=1/2
	5508.1	Ne (3G)	1.318[−1]	$2s^2 2p^6$ J=0 – $2s^2 2p_-^2 2p_+^3 3s$ J=1
	5629.4	F	4.338[−3]	$2s 2p^6$ J=1/2 – $2s^2 2p_-^1 2p_+^3 3p_-$ J=3/2 [c]

[a] enabled by mixing between $2s^2 2p^5 3s 3d + 2s^2 2p^5 3p^2$

[b] enabled by mixing between $2s 2p^4 3s + 2s 2p^4 3d + 2s^2 2p^3 3p$

[c] enabled by mixing between $2s^2 2p^4 3p + 2s 2p^5 3s + 2s 2p^5 3d$

TABLE VII. $2-3$ transitions in neonlike Zr^{30+} and associated satellites. The legend is the same as in Table V.

λ_E	λ_{Th}	Ion (Label)	gf	Transition
	5041.2	F	2.512[+0]	$2s^2 2p^5$ J=3/2 – $2s^2 2p_-^1 2p_+^3 3d_-$ J=5/2
	5044.1	F	1.774[+0]	$2s^2 2p^5$ J=3/2 – $2s^2 2p_-^1 2p_+^3 3d_-$ J=3/2
	5080.7	F	8.442[−1]	$2s^2 2p^5$ J=3/2 – $2s^2 2p_-^1 2p_+^3 3d_-$ J=5/2
	5198.1	F	1.442[+0]	$2s^2 2p^5$ J=3/2 – $2s^2 2p_-^2 2p_+^2 3d_+$ J=5/2
5200.4	5199.0	Ne (3C)	1.741[+0]	$2s^2 2p^6$ J=0 – $2s^2 2p_-^1 2p_+^4 3d_-$ J=1
5207.5	5205.9	Na	8.601[−1]	$2s^2 2p^6 3s$ J=1/2 – $2s^2 2p_-^1 2p_+^4 3s 3d_-$ J=3/2
5212.3	5210.9	F	7.467[−1]	$2s^2 2p^5$ J=3/2 – $2s^2 2p_-^2 2p_+^2 3d_-$ J=3/2
5227.7	5228.2	F	1.815[+0]	$2s^2 2p^5$ J=3/2 – $2s^2 2p_-^2 2p_+^2 3d_+$ J=5/2
	5238.6	F	8.436[−1]	$2s^2 2p^5$ J=3/2 – $2s^2 2p_-^2 2p_+^2 3d_+$ J=3/2
5241.2	5241.3	Na	1.165[+0]	$2s^2 2p^6 3s$ J=1/2 – $2s^2 2p_-^1 2p_+^4 3s 3d_-$ J=1/2
5248.1	5249.1	Na	1.327[+0]	$2s^2 2p^6 3s$ J=1/2 – $2s^2 2p_-^2 2p_+^3 3s 3d_+$ J=3/2
5263.1	5264.8	Mg	1.708[+0]	$2s^2 2p^6 3s^2$ J=0 – $2s^2 2p_-^1 2p_+^4 3s^2 3d_-$ J=1
5375.8	5375.0	Ne (3D)	1.776[+0]	$2s^2 2p^6$ J=0 – $2s^2 2p_-^2 2p_+^3 3d_+$ J=1
5390.2	5392.0	F	1.886[−1]	$2s^2 2p^5$ J=3/2 – $2s^2 2p_-^1 2p_+^3 3s$ J=5/2
5396.2	5393.7	Na	9.197[−1]	$2s^2 2p^6 3s$ J=1/2 – $2s^2 2p_-^2 2p_+^3 3p_+^2$ J=3/2 [a]
5403.1	5402.1	Na	8.023[−1]	$2s^2 2p^6 3s$ J=1/2 – $2s^2 2p_-^2 2p_+^3 3s 3d_+$ J=1/2
5430.6	5429.1	Na	1.042[+0]	$2s^2 2p^6 3s$ J=1/2 – $2s^2 2p_-^1 2p_+^4 3p_- 3p_+$ J=3/2[a]
5441.5	5445.4	Mg	1.812[+0]	$2s^2 2p^6 3s^2$ J=0 – $2s^2 2p_-^2 2p_+^3 3s^2 3d_+$ J=1
	5624.1	F	2.507[−1]	$2s^2 2p^5$ J=3/2 – $2s^2 2p_-^2 2p_+^2 3s$ J=3/2
	5638.5	F	4.769[−2]	$2s^2 2p^5$ J=3/2 – $2s^2 2p_-^2 2p_+^2 3s$ J=5/2
	5699.6	Na	4.630[−2]	$2s^2 2p^6 3p$ J=3/2 – $2s^2 2p_-^1 2p_+^4 3s 3p_-$ J=1/2
	5968.5	F	4.971[−3]	$2s 2p^6$ J=1/2 – $2s^2 2p_-^1 2p_+^3 3p_-$ J=3/2 [b]

[a] enabled by mixing between $2s^2 2p^5 3s^2 + 2s^2 2p^5 3s 3d + 2s^2 2p^5 3p^2$

[b] enabled by mixing between $2s 2p^5 3s + 2s 2p^5 3d + 2s^2 2p^4 3p$

TABLE VIII. $2-4$, $2-5$, $2-6$, $2-7$, $2-8$ and $2-9$ transitions in neonlike Kr^{26+} and associated satellites. The legend is the same as in Table V.

λ_E	λ_{Th}	Ion (Label)	gf	Transition
4339.2	4340.1	Ne (9C)	2.205[−2]	$2s^22p^6$ J=0 – $2s^22p_-^12p_+^49d_-$ J=1
4359.3	4351.7	F	9.467[−2]	$2s^22p^5$ J=3/2 – $2s^22p_-^22p_+^27d_+$ J=5/2
4387.2	4391.0	Ne (8C)	2.750[−2]	$2s^22p^6$ J=0 – $2s^22p_-^12p_+^48d_-$ J=1
4423.5	4425.3	Ne (9D)	4.260[−2]	$2s^22p^6$ J=0 – $2s^22p_-^22p_+^39d_+$ J=1
4464.5	4467.3	Ne (7C)	4.416[−2]	$2s^22p^6$ J=0 – $2s^22p_-^12p_+^47d_-$ J=1
4475.6	4475.5	Ne (8D)	4.215[−2]	$2s^22p^6$ J=0 – $2s^22p_-^22p_+^38d_+$ J=1
4475.6	4477.0	F	1.572[−1]	$2s^22p^5$ J=3/2 – $2s^22p_-^22p_+^26d_+$ J=5/2
4475.6	4477.2	F	9.090[−2]	$2s^22p^5$ J=3/2 – $2s^22p_-^22p_+^26d_+$ J=3/2
4488.1	4487.1	O	3.746[−1]	$2s^22p_-^22p_+^2$ J=2 – $2s^22p_-^22p_+^15d_+$ J=3
4497.0	4495.9	O	1.942[−1]	$2s^22p_-^12p_+^3$ J=1 – $2s^22p_-^12p_+^25d_+$ J=2
4497.0	4496.0	O	2.868[−1]	$2s^22p_-^12p_+^3$ J=2 – $2s^22p_-^12p_+^25d_+$ J=3
4497.0	4496.0	O	1.848[−1]	$2s^22p_-^12p_+^3$ J=2 – $2s^22p_-^12p_+^25d_+$ J=2
4497.0	4496.9	O	6.168[−2]	$2s^22p_-^12p_+^3$ J=2 – $2s^22p_-^12p_+^25d_+$ J=1
4516.4	4512.4	Ne (5A)	4.685[−2]	$2s^22p^6$ J=0 – $2s2p^65p_+$ J=1
4520.5	4517.3	Ne (5B)	1.549[−2]	$2s^22p^6$ J=0 – $2s2p^65p_-$ J=1
4554.7	4554.3	Ne (7D)	7.860[−2]	$2s^22p^6$ J=0 – $2s^22p_-^22p_+^37d_+$ J=1
4588.2	4588.1	Ne (6C)	5.829[−2]	$2s^22p^6$ J=0 – $2s^22p_-^12p_+^46d_-$ J=1
4591.6	4592.6	F	9.077[−2]	$2s^22p^5$ J=3/2 – $2s^22p_-^12p_+^35d_-$ J=3/2
4591.6	4592.8	F	6.640[−2]	$2s^22p^5$ J=3/2 – $2s^22p_-^12p_+^35d_-$ J=1/2
4613.7	4614.9	F	1.059[−1]	$2s^22p^5$ J=3/2 – $2s^22p_-^12p_+^35d_-$ J=5/2
	4651.5	Na	1.182[−2]	$2s^22p^63s$ J=1/2 – $2s^22p_-^22p_+^33s_+7d_+$ J=3/2
	4668.3	F	9.498[−2]	$2s^22p^5$ J=3/2 – $2s^22p_-^22p_+^25d_+$ J=5/2
4682.1	4684.8	Ne (6D)	1.205[−1]	$2s^22p^6$ J=0 – $2s^22p_-^22p_+^36d_+$ J=1
4701.0	4702.0	F	2.859[−1]	$2s^22p^5$ J=3/2 – $2s^22p_-^22p_+^25d_+$ J=5/2

4701.0	4702.6	F	1.655[−1]	$2s^22p^5$ J=3/2 – $2s^22p_-^22p_+^25d_+$ J=3/2
	4770.7	Mg	4.343[−2]	$2s^22p^63s^2$ J=0 – $2s^22p_-^12p_+^43s^26d_-$ J=1
4775.9	4776.7	Na	1.091[−1]	$2s^22p^63s$ J=1/2 – $2s^22p_-^22p_+^33s_+6d_+$ J=3/2
	4781.8	Na	5.822[−2]	$2s^22p^63s$ J=1/2 – $2s^22p_-^22p_+^33s_+6d_+$ J=1/2
4809.0	4809.1	Ne (5C)	1.367[−1]	$2s^22p^6$ J=0 – $2s^22p_-^12p_+^45d_-$ J=1
	4818.1	F	9.164[−2]	$2s^22p^5$ J=3/2 – $2s2p_-^22p_+^34p_+$ J=5/2
	4819.1	F	1.062[−1]	$2s^22p^5$ J=3/2 – $2s2p_-^22p_+^34p_+$ J=3/2
	4848.9	O	3.808[−1]	$2s^22p_-^22p_+^2$ J=2 – $2s^22p_-^12p_+^24d_-$ J=2
	4851.1	O	3.412[−1]	$2s^22p_-^22p_+^2$ J=2 – $2s^22p_-^12p_+^24d_-$ J=3
	4851.5	O	2.683[−1]	$2s^22p_-^22p_+^2$ J=0 – $2s^22p_-^12p_+^24d_-$ J=1
	4871.9	Mg	1.098[−1]	$2s^22p^63s^2$ J=0 – $2s^22p_-^22p_+^33s^26d_+$ J=1
	4875.0	O	2.114[−1]	$2s^22p_-^22p_+^2$ J=2 – $2s^22p_-^12p_+^24d_-$ J=3
	4878.2	O	1.244[−1]	$2s^22p_-^22p_+^2$ J=2 – $2s^22p_-^12p_+^24d_-$ J=2
4896.7	4896.5	Na	7.576[−2]	$2s^22p^63s$ J=1/2 – $2s^22p_-^12p_+^43s_+5d_-$ J=1/2,3/2
4896.7	4896.5	Na	1.068[−1]	$2s^22p^63s$ J=1/2 – $2s^22p_-^12p_+^43s_+5d_-$ J=3/2
4912.3	4910.8	Ne (5D)	2.327[−1]	$2s^22p^6$ J=0 – $2s^22p_-^22p_+^35d_+$ J=1
4958.5	4951.6	Ne (4A)	1.167[−1]	$2s^22p^6$ J=0 – $2s2p^64p_+$ J=1
4964.7	4957.2	O	8.525[−1]	$2s^22p_-^22p_+^2$ J=2 – $2s^22p_-^22p_+^14d_+$J=3
4968.2	4962.2	Ne (4B)	1.297[−2]	$2s^22p^6$ J=0 – $2s2p^64p_-$ J=1
	4963.1	O	1.661[−1]	$2s^22p_-^22p_+^2$J=2 – $2s^22p_-^22p_+^14d_+$J=2
4972.6	4970.2	Ne (5G)	3.334[−2]	$2s^22p^6$ J=0 –$2s^22p_-^22p_+^35s_+$J=1
4982.9	4980.4	Mg	1.077[−1]	$2s^22p^63s^2$ J=0 – $2s^22p_-^12p_+^43s^25d_-$ J=1
4999.6	4999.4	O	2.346[−1]	$2s^22p_-^22p_+^2$ J=0 – $2s^22p_-^22p_+^14d_+$ J=1
4999.6	5001.1	Na	2.563[−1]	$2s^22p^63s$ J=1/2 – $2s^22p_-^22p_+^33s_+5d_+$ J=3/2
5003.6	5004.3	Na	7.252[−2]	$2s^22p^63s$ J=1/2 – $2s^22p_-^22p_+^33s_+5d_-$ J=1/2
5026.3	5029.0	O	6.089[−1]	$2s2p_-^22p_+^3$ J=2 – $2s2p_-^22p_+^24d_+$ J=3
5027.8	5018.3	Na	1.333[−1]	$2s^22p^63s$ J=1/2 – $2s2p^63s_+4p_+$ J=3/2

5055.2	5053.8	F	2.890[−1]	$2s^2 2p^5$ J=3/2 – $2s^2 2p^1_- 2p^3_+ 4d_-$ J=5/2
5055.2	5055.3	F	2.709[−1]	$2s^2 2p^5$ J=3/2 – $2s^2 2p^1_- 2p^3_+ 4d_-$ J=3/2
5055.2	5056.3	F	1.739[−1]	$2s^2 2p^5$ J=3/2 – $2s^2 2p^1_- 2p^3_+ 4d_-$ J=1/2
5084.0	5082.4	F	2.427[−1]	$2s^2 2p^5$ J=3/2 – $2s^2 2p^1_- 2p^3_+ 4d_-$ J=5/2
	5089.8	Mg	2.308[−1]	$2s^2 2p^6 3s^2$ J=0 – $2s^2 2p^2_- 2p^3_+ 3s^2 5d_+$ J=1
5131.6	5129.4	O	4.720[−2]	$2s 2p^2_- 2p^3_+$ J=2 – $2s 2p^2_- 2p^2_+ 4s$ J=2
5148.8	5146.2	F	2.254[−1]	$2s^2 2p^5$ J=3/2 – $2s^2 2p^2_- 2p^2_+ 4d_+$ J=5/2
5165.0	5163.8	F	4.248[−1]	$2s^2 2p^5$ J=1/2 – $2s^2 2p^1_- 2p^3_+ 4d_+$ J=3/2
5173.9	5171.9	F	4.999[−2]	$2s^2 2p^5$ J=1/2 – $2s^2 2p^1_- 2p^3_+ 4d_-$ J=3/2
5173.9	5172.9	F	1.559[−2]	$2s^2 2p^5$ J=1/2 – $2s^2 2p^1_- 2p^3_+ 4d_-$ J=1/2
5181.6	5183.2	F	6.674[−1]	$2s^2 2p^5$ J=3/2 – $2s^2 2p^2_- 2p^2_+ 4d_+$ J=5/2
5184.1	5184.2	F	3.289[−1]	$2s^2 2p^5$ J=3/2 – $2s^2 2p^2_- 2p^2_+ 4d_+$ J=3/2
5195.4	5190.8	F	9.473[−2]	$2s^2 2p^5$ J=3/2 – $2s^2 2p^2_- 2p^2_+ 4d_+$ J=1/2
5195.4	5192.5	F	3.229[−2]	$2s 2p^6$ J=1/2 – $2s^2 2p^2_- 2p^2_+ 4p_+$ J=3/2 [a]
5195.4	5195.2	F	1.916[−1]	$2s^2 2p^5$ J=1/2 – $2s^2 2p^1_- 2p^3_+ 4d_+$ J=3/2
5278.7	5278.4	Ne (4C)	3.302[−1]	$2s^2 2p^6$ J=0 – $2s^2 2p^1_- 2p^4_+ 4d_-$ J=1
	5317.7	Na	5.822[−2]	$2s^2 2p^6 3p_-$ J=1/2 – $2s^2 2p^1_- 2p^4_+ 3p_- 4d_-$ J=3/2
5356.7	5357.2	Na	1.864[−1]	$2s^2 2p^6 3s$ J=1/2 – $2s^2 2p^1_- 2p^4_+ 3s_+ 4d_-$ J=1/2
5356.7	5358.9	Na	5.822[−2]	$2s^2 2p^6 3s$ J=1/2 – $2s^2 2p^1_- 2p^4_+ 3s_+ 4d_-$ J=3/2
5361.2	5360.7	Na	5.342[−1]	$2s^2 2p^6 3p_+$ J=3/2 – $2s^2 2p^1_- 2p^4_+ 3p_+ 4d_-$ J=5/2
5368.9	5369.1	Na	2.423[−1]	$2s^2 2p^6 3p_-$ J=1/2 – $2s^2 2p^1_- 2p^4_+ 3p_- 4d_-$ J=3/2
5375.5				
5396.4	5396.7	Ne (4D)	4.335[−1]	$2s^2 2p^6$ J=0 – $2s^2 2p^2_- 2p^3_+ 4d_+$ J=1
5407.3	5409.0	Ne (4F)	6.796[−2]	$2s^2 2p^6$ J=0 – $2s^2 2p^1_- 2p^4_+ 4s_+$ J=1
5436.6	5426.1	Mg	3.053[−1]	$2s^2 2p^6 3s^2$ J=0 – $2s^2 2p^1_- 2p^4_+ 3s^2 4d_-$ J=1
5477.7	5479.8	Na	5.506[−1]	$2s^2 2p^6 3s$ J=1/2 – $2s^2 2p^2_- 2p^3_+ 3s_+ 4d_+$ J=3/2
5482.3	5484.4	Na	2.191[−1]	$2s^2 2p^6 3s$ J=1/2 – $2s^2 2p^2_- 2p^3_+ 3s_+ 4d_+$ J=1/2

5487.0	5488.3	Na	5.194[−1]	$2s^2 2p^6 3p_-$ J=1/2 – $2s^2 2p_-^2 2p_+^3 3p_- 4d_+$ J=3/2
5561.5?	5540.6	Ne (4G)	2.465[−2]	$2s^2 2p^6$ J=0 – $2s^2 2p_-^2 2p_+^3 4s_+$ J=1
	5551.9	Mg	4.550[−1]	$2s^2 2p^6 3s^2$ J=0 – $2s^2 2p_-^2 2p_+^3 3s^2 4d_+$ J=1

[a] enabled by mixing between $2s2p^5 4s$ + $2s2p^5 4d$ + $2s^2 2p^4 4p$

FIGURES

FIG. 1. The Kr^{26+} $2-3$ spectrum with satellites (composite over several similar discharges) is shown in the top frame, including the neonlike transition designations. In the bottom frame is a synthetic spectrum with neonlike krypton shown by the solid black line, fluorinelike by the purple dash-dot line, sodiumlike by the red dotted line and magnesiumlike by the green dashed line.

FIG. 2. The spectrum in the vicinity of the Kr^{26+} 3C ($2p_- - 3d_-$) transition, with the same legend as for the bottom frame of Fig.1. Helium-like Si calibration lines w and z are shown by the vertical dotted lines at 6648.18 and 6740.50 mÅ.

FIG. 3. Neonlike 3C transitions and long wavelength satellites for five elements, from the top: palladium, molybdenum, niobium, zirconium and krypton. The Kr^{26+} $2p_- - 4d_-$ line at 5178.7 mÅ is visible in the zirconium spectrum; the palladium line at 3774.6 mÅ in the top spectrum is unidentified.

FIG. 4. The wavelength differences between satellites and the neonlike 3C transitions as a function of the atomic charge of the neonlike ion. Purple dots represent Mg-like $3d_-$ J=1, green $\times$s are for Na-like $3d_-$ J=$\frac{3}{2}$ and red +s are for Na-like $3d_-$ J=$\frac{1}{2}$. The solid lines represent the calculated differences.

FIG. 5. The $2p_+ - 3s_+$ ΔJ=1 (3G) and ΔJ=2 (M2) transitions in neonlike molybdenum (top) and krypton (bottom), including sodiumlike satellites. The solid black curves are synthetic Ne-like spectra from collisional-radiative modeling and the red dotted curves are the calculated Na-like spectra.

FIG. 6. The calculated intensity ratio of the M2 and 3G transitions in neonlike molybdenum (green) and krypton (red) as a function electron density (curves), along with the measured values. Green dot: Mo, red asterisk: Kr.

FIG. 7. Spectra in the vicinity of the neonlike 3F transitions in molybdenum (top) and krypton (bottom), including the E22 ($2p_+ - 3p_+$) and E23 ($2p_+ - 3p_-$) lines, and nearby satellites. Simulated spectra are also shown, with the same legend as in the bottom of Fig.1.

FIG. 8. Spectra including the neonlike 2s - $3d_+$ and 2s - $3p_+$ transitions in molybdenum (top) and krypton (bottom), along with nearby satellites. Simulated spectra are also shown, with the same legend as in the bottom of Fig.1. Also visible in these spectra are calibration lines, S^{14+} Ly_β at 4299.2 mÅ (top) and the Si^{13+} Ly_α doublet at 6180.44 and 6185.85 mÅ.

FIG. 9. The spectrum in the vicinity of Mo^{32+} 3A and 3B, which includes the bright Fl-like $2p_-$ − $3d_-$ transition. The location of the Cl^{15+} resonance line at 4444.58 mÅ, used for the wavelength calibration, is indicated by the dotted vertical line. The synthetic spectrum is also shown, which includes the O-like transitions depicted by the green dash-dot-dot-dot line.

FIG. 10. The spectrum of the Kr^{26+} 4C, 4D and 4F transitions, with Na- and Mg-like $2p_-$ − $4d_-$ satellites. Also shown is the synthetic collisional radiative synthetic spectrum, with Ne-like lines shown in black, Na-like transitions depicted by the red dotted lines and the Mg-like $2p_-$ − $4d_-$ transition shown as the green dashed line.

FIG. 11. The n=4 and n=5 energy level diagrams for Mo^{32+} (top) and Kr^{26+} (bottom) with the left ordinates expressed in the transition (to the ground state) wavelengths and the right ordinates in eV. Upper levels for p, s and d are on the left in purple, in the center in green and on the right in red, respectively. Measured transition wavelengths (to the ground state) are given for each of the upper levels, with unobserved theoretical wavelengths in parentheses.

FIG. 12. Calculated oscillator strengths for neonlike nF $2p_-$ − ns_+ (top) and nG $2p_+$ − ns_- (bottom) transitions as a function of n for molybdenum (green dots), niobium (purple boxes), zirconium (black ×s) and krypton (red asterisks).

FIG. 13. Intensity ratios of neonlike 4F ($2p_- - 4s_+$) to 4D ($2p_+ - 4d_+$) transitions as a function of the upper level energy separations, with the calculations shown as the green dots and the measured points as the red asterisks.

FIG. 14. A composite spectrum of high n transitions in Kr^{26+}, up to n=9, with Fl-like satellites, and Cl^{15+} calibration lines is shown in the top frame. In the bottom frame is a synthetic spectrum, with Ne-like shown as the black line, Na-like as the red dotted line and Fl-like as the purple dash-dot line.

FIG. 15. The energy level separation in eV between np_+ and np_- as a function of n. Green diamonds represent Mo^{32+} theory, green boxes are for Kr^{26+} theory, red dots are for Mo^{32+} experiment and red $\times$s represent Kr^{26+} experiment.

FIG. 16. Neonlike 2s - np oscillator strengths as a function of n, for molybdenum: green dots, niobium: purple boxes and krypton: red asterisks.

FIG. 17. Spectra including the neonlike 4A, 4B and 5G transitions in Mo^{32+} (top) and Kr^{26+} (bottom), with nearby satellites. Synthetic spectra are also shown with Ne-like given as solid black lines and Na-like as red dotted lines.

FIG. 18. The brightness ratios of nA to nB (2s - np_+ to 2s - np_-) as a function of n for Mo^{32+} (green dots) and Kr^{26+} (red asterisks). Calculated curves are also shown.

FIG. 19. Spectra including the neonlike 7D, 6C, 5A and 5B transitions in Mo^{32+} (top) and Kr^{26+} (bottom), with nearby satellites. Synthetic spectra are also shown with Ne-like represented by solid black lines, Na-like given as red dotted lines, Fl-like as purple dash-dot lines and O-like as green dash-dot-dot-dot lines.

FIG. 20. The intensity ratios of Ne-like 7D to 6C transitions as a function of energy level separation. Calculations are shown as green dots, measurements are represented as red asterisks.

FIG. 21. The calculated CR intensity ratios of Ne-like E22/3F (top) and E23/3F (bottom) transitions as a function of upper level energy separation are shown as green dots, with observations shown as red asterisks.

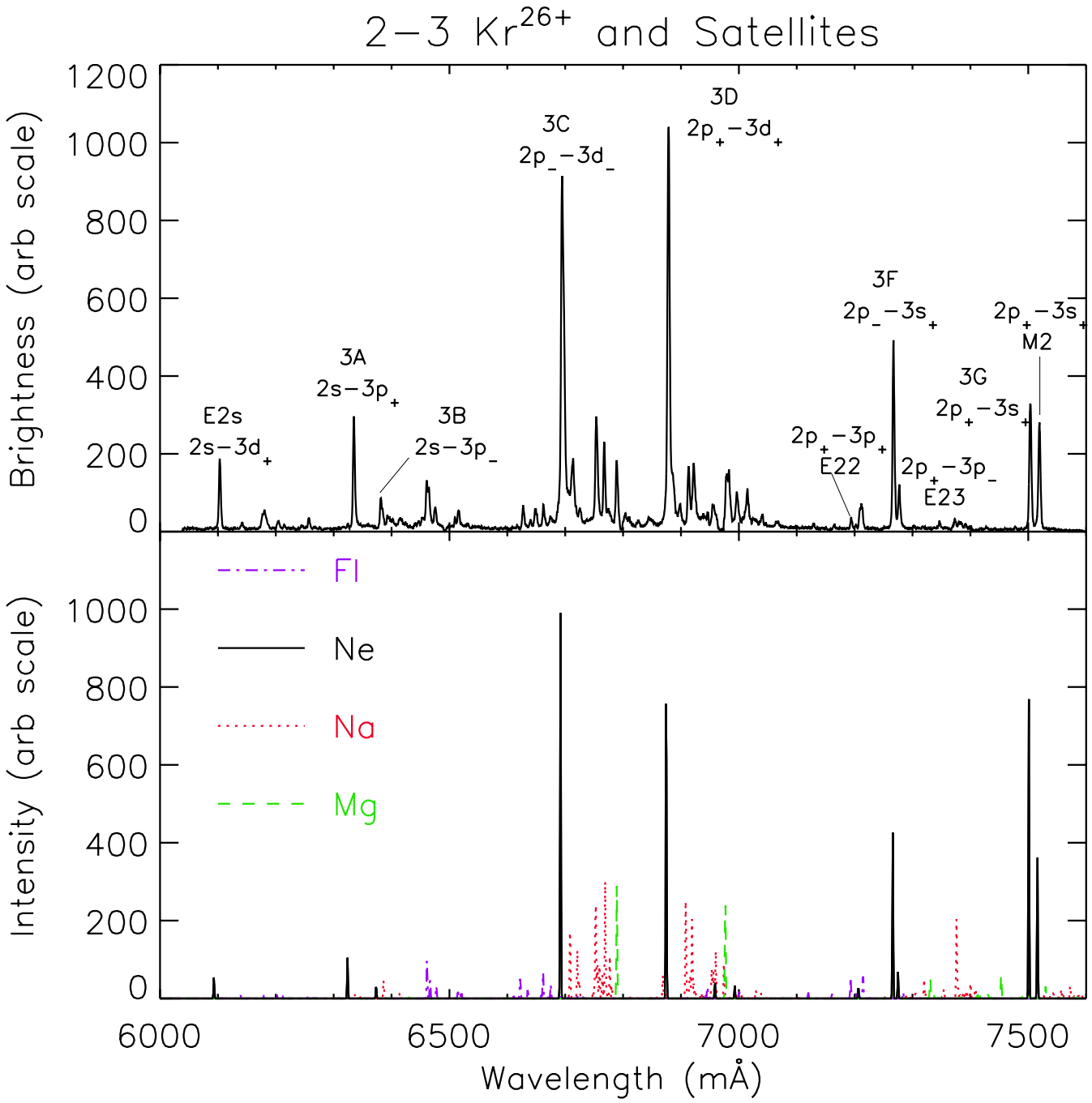
2−3 Kr26+ and Satellites
Brightness (arb scale)
1200
1000
800
600
400
200
0
E2s
2s−3d+
3A
2s−3p+
3B
2s−3p−
3C
2p−−3d−
3D
2p+−3d+
2p+−3p+
E22
3F
2p−−3s+
2p+−3p−
E23
3G
2p+−3s+
M2
2p+−3s+
Fl
Ne
Na
Mg
Intensity (arb scale)
1000
800
600
400
200
0
6000
6500
7000
7500
Wavelength (mÅ)

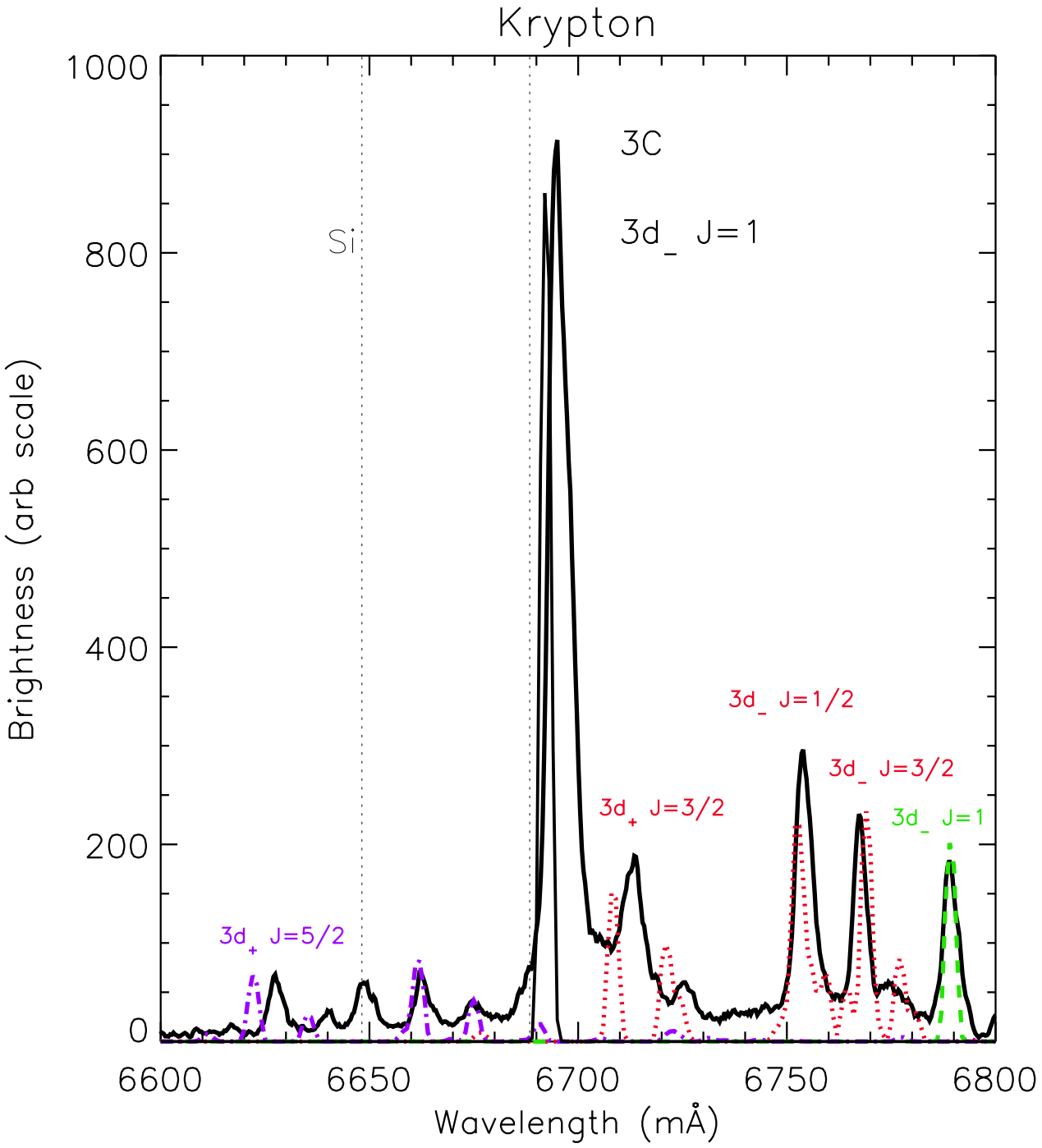
Krypton
3C
3d_ J=1
Si
3d+ J=5/2
3d+ J=3/2
3d_ J=1/2
3d_ J=3/2
3d_ J=1
Brightness (arb scale)
Wavelength (mÅ)
0
200
400
600
800
1000
6600
6650
6700
6750
6800

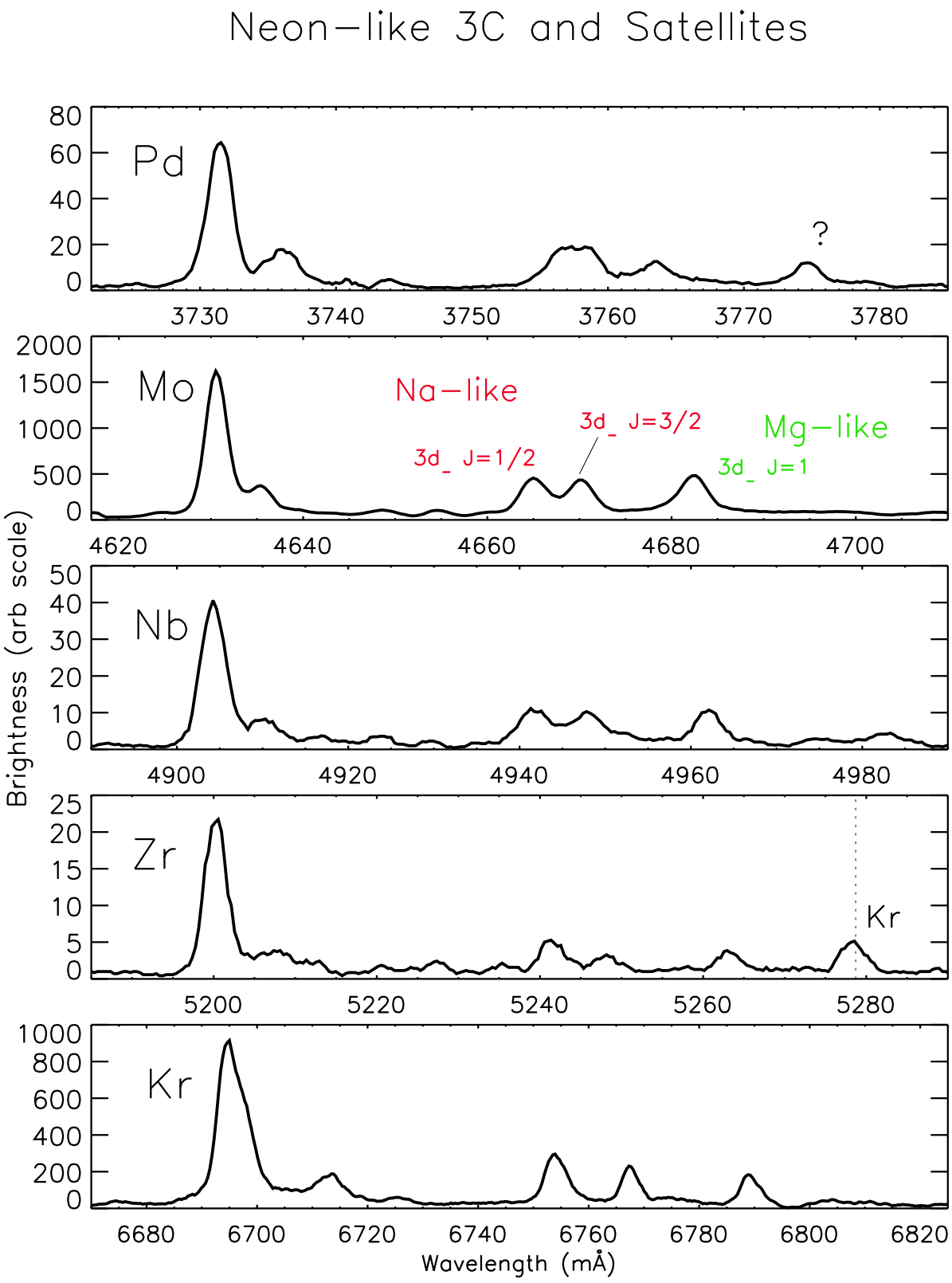
Neon−like 3C and Satellites
Pd
?
Mo
Na−like
3d_ J=1/2
3d_ J=3/2
Mg−like
3d_ J=1
Nb
Zr
Kr
Kr
Brightness (arb scale)
Wavelength (mÅ)

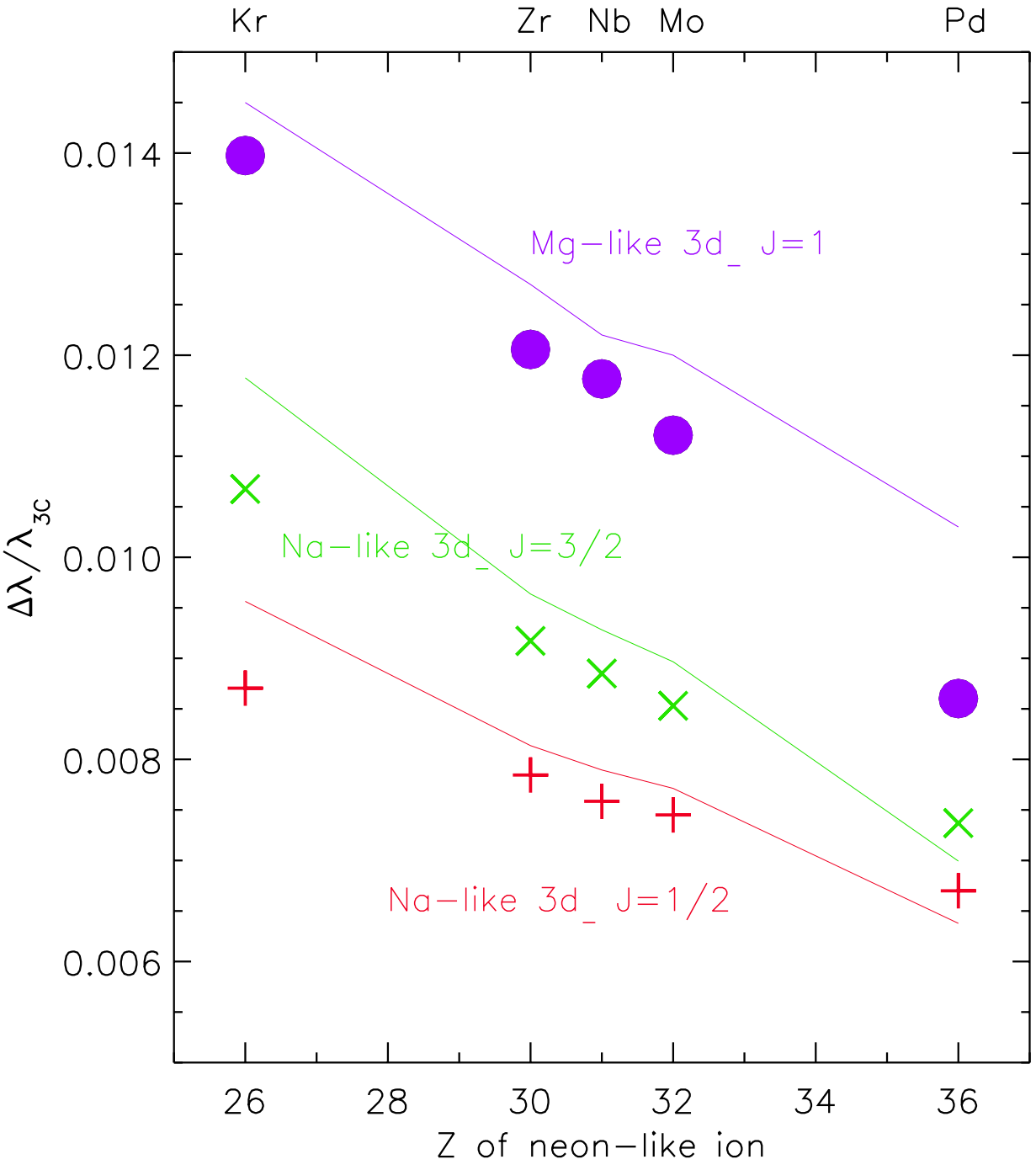
Wavelength Differences between Satellites and
Neon−like 3C (2p_−3d_) Transitions
Kr
Zr
Nb
Mo
Pd
0.014
0.012
0.010
0.008
0.006
Δλ/λ3C
Mg−like 3d_ J=1
Na−like 3d_ J=3/2
Na−like 3d_ J=1/2
26
28
30
32
34
36
Z of neon−like ion

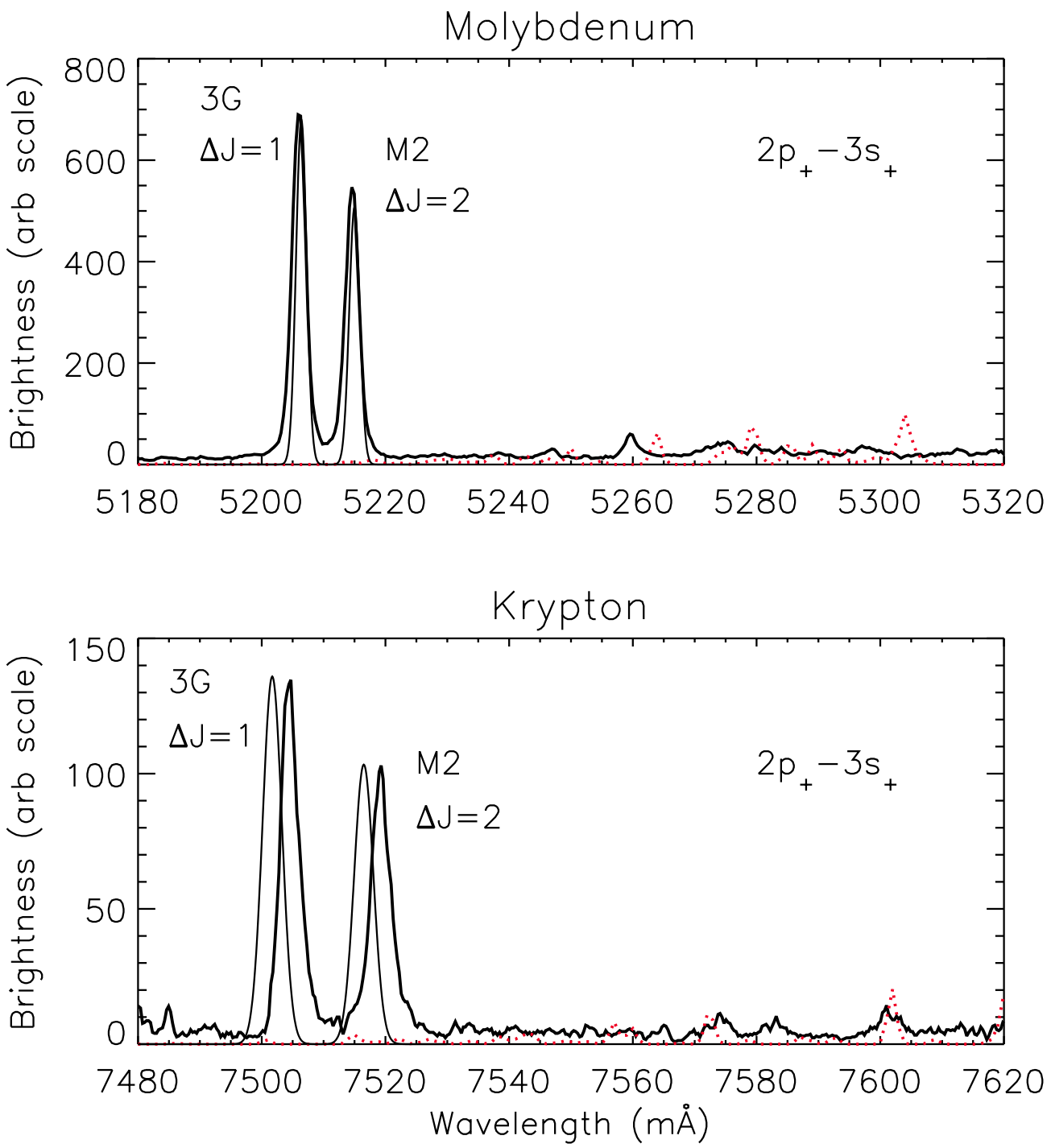
Molybdenum
Brightness (arb scale)
800
600
400
200
0
3G
ΔJ=1
M2
ΔJ=2
2p+−3s+
5180
5200
5220
5240
5260
5280
5300
5320
Krypton
Brightness (arb scale)
150
100
50
0
3G
ΔJ=1
M2
ΔJ=2
2p+−3s+
7480
7500
7520
7540
7560
7580
7600
7620
Wavelength (mÅ)

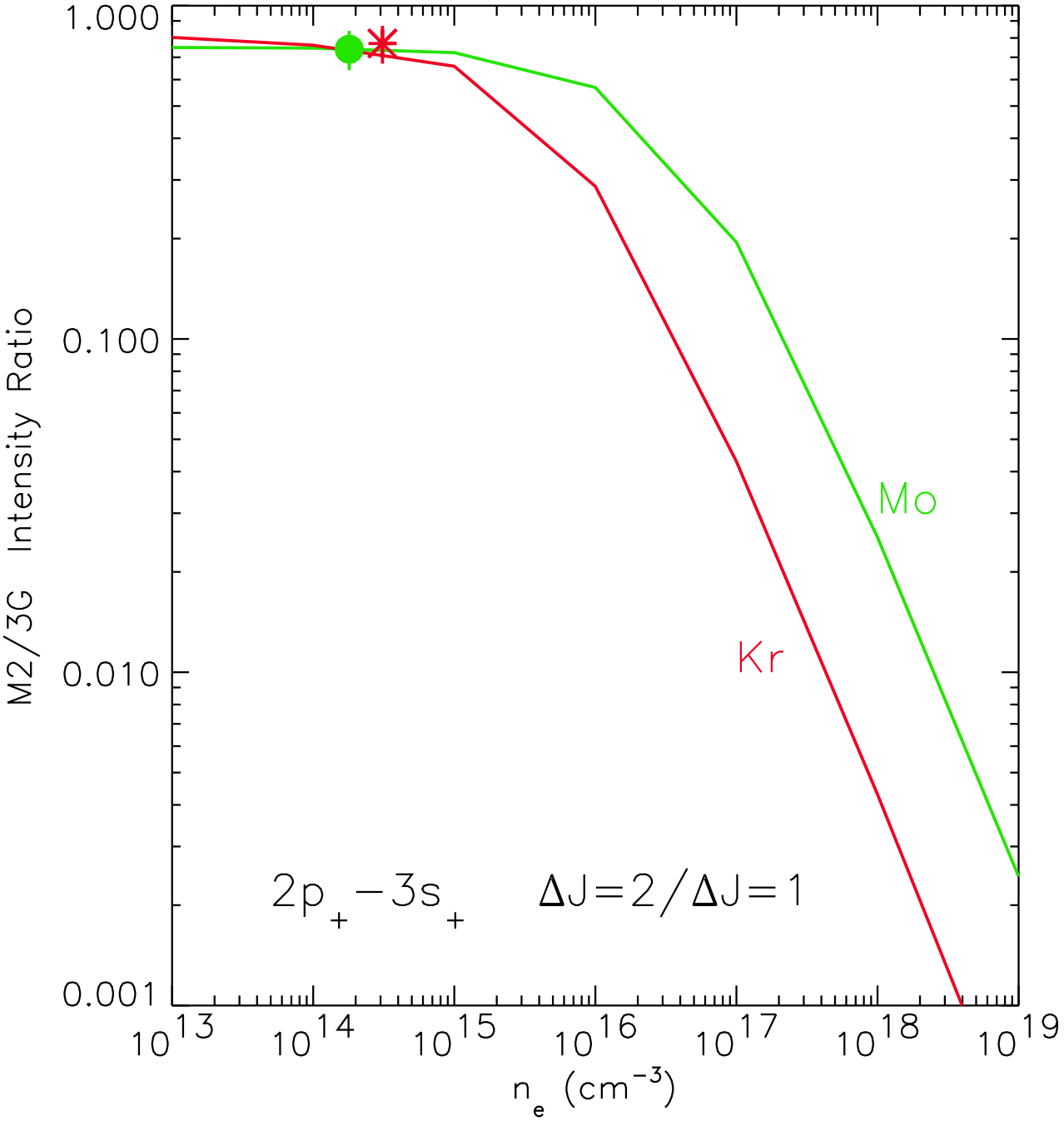
1.000
0.100
0.010
0.001
M2/3G Intensity Ratio
Mo
Kr
2p+ − 3s+ ΔJ=2/ΔJ=1
10^13
10^14
10^15
10^16
10^17
10^18
10^19
ne (cm^-3)

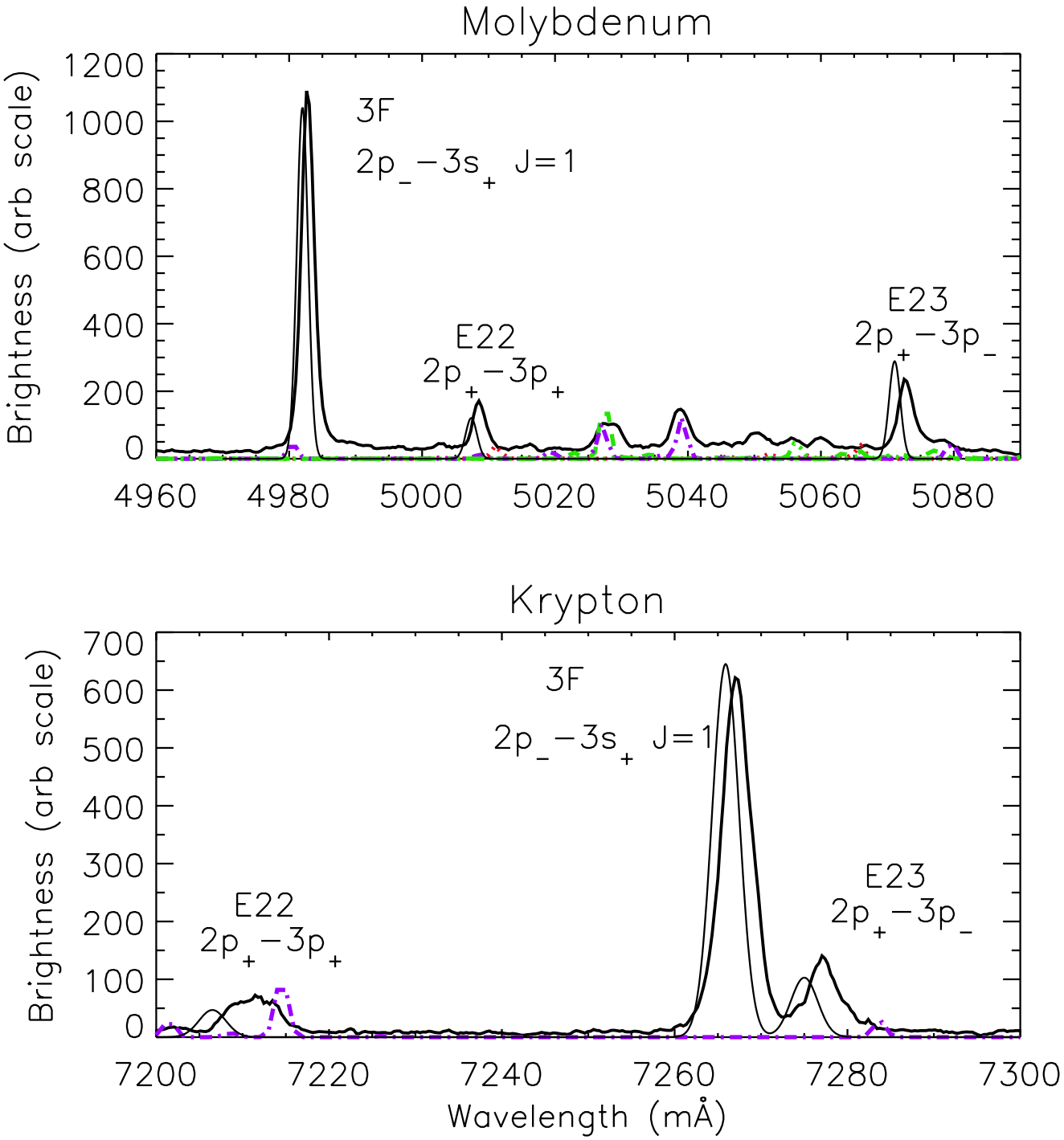
Molybdenum
Brightness (arb scale)
1200
1000
800
600
400
200
0
3F
2p_ − 3s_+ J=1
E22
2p_+ − 3p_+
E23
2p_+ − 3p_−
4960
4980
5000
5020
5040
5060
5080
Krypton
Brightness (arb scale)
700
600
500
400
300
200
100
0
3F
2p_ − 3s_+ J=1
E22
2p_+ − 3p_+
E23
2p_+ − 3p_−
7200
7220
7240
7260
7280
7300
Wavelength (mÅ)

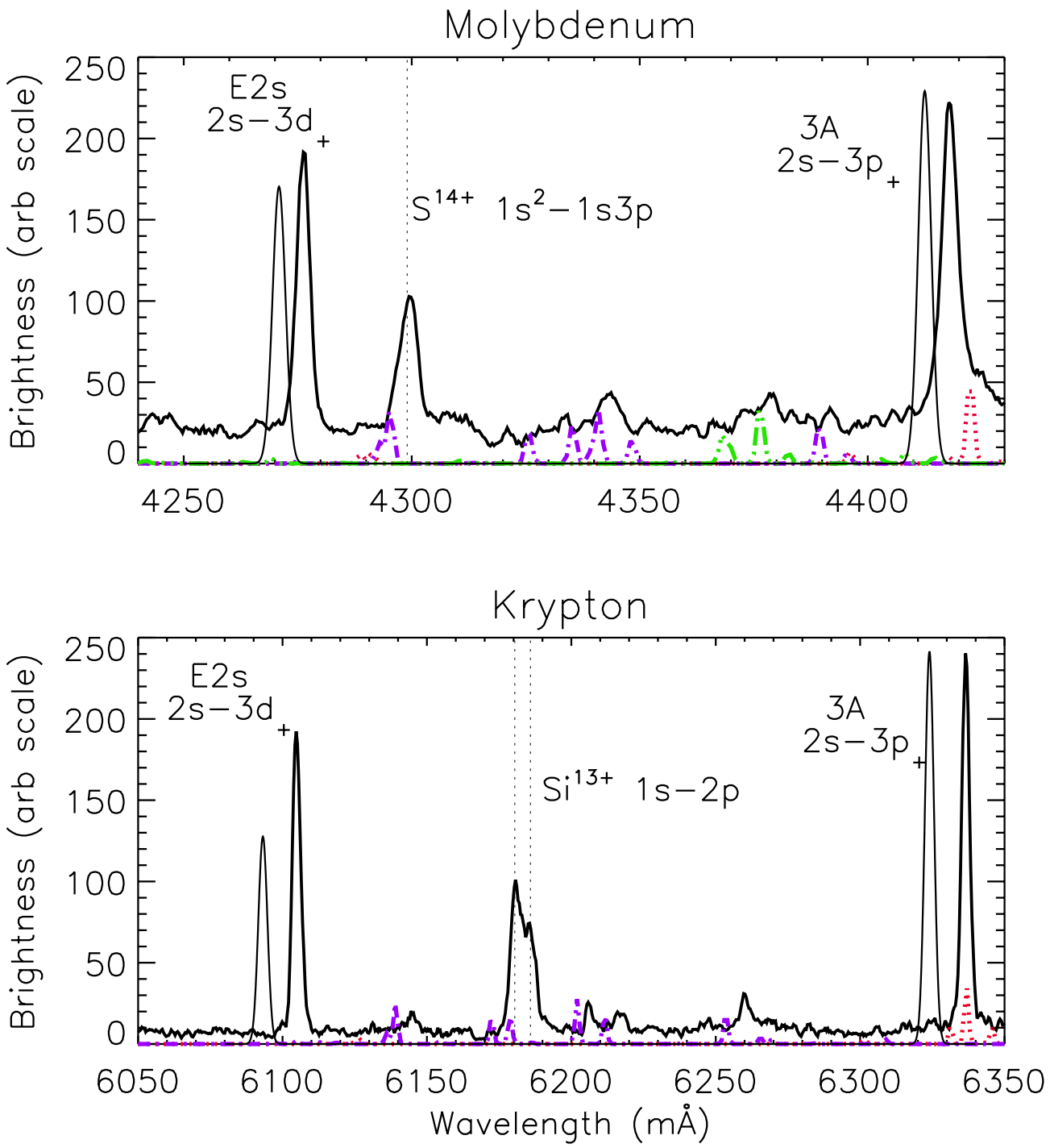
Molybdenum
Brightness (arb scale)
250
200
150
100
50
0
E2s
2s−3d+
S14+ 1s2−1s3p
3A
2s−3p+
4250
4300
4350
4400
Krypton
Brightness (arb scale)
250
200
150
100
50
0
E2s
2s−3d+
Si13+ 1s−2p
3A
2s−3p+
6050
6100
6150
6200
6250
6300
6350
Wavelength (mÅ)

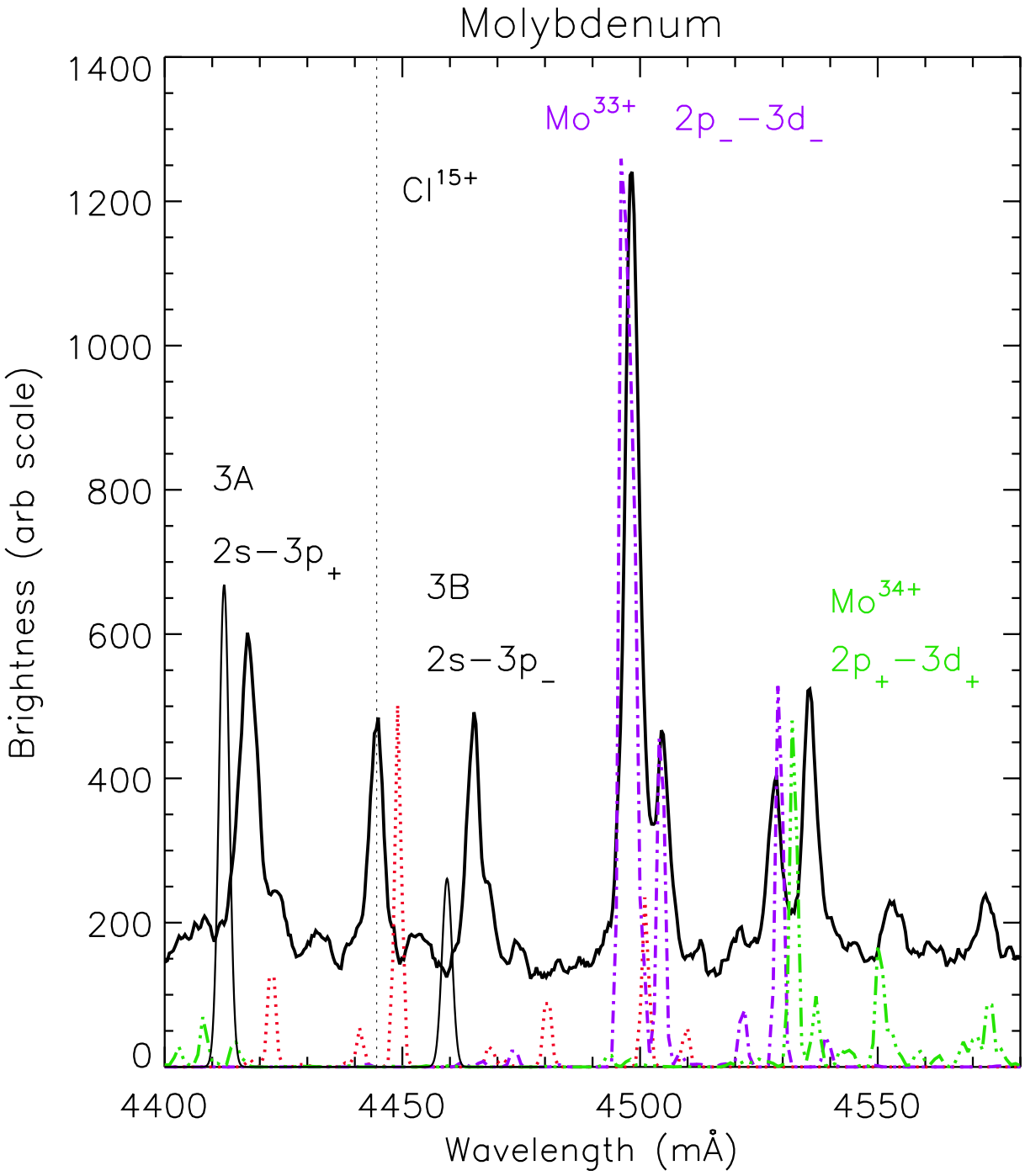
Molybdenum
1400
1200
1000
800
600
400
200
0
Brightness (arb scale)
4400
4450
4500
4550
Wavelength (mÅ)
Mo33+ 2p_−3d_
Cl15+
3A
2s−3p+
3B
2s−3p_
Mo34+
2p+−3d+

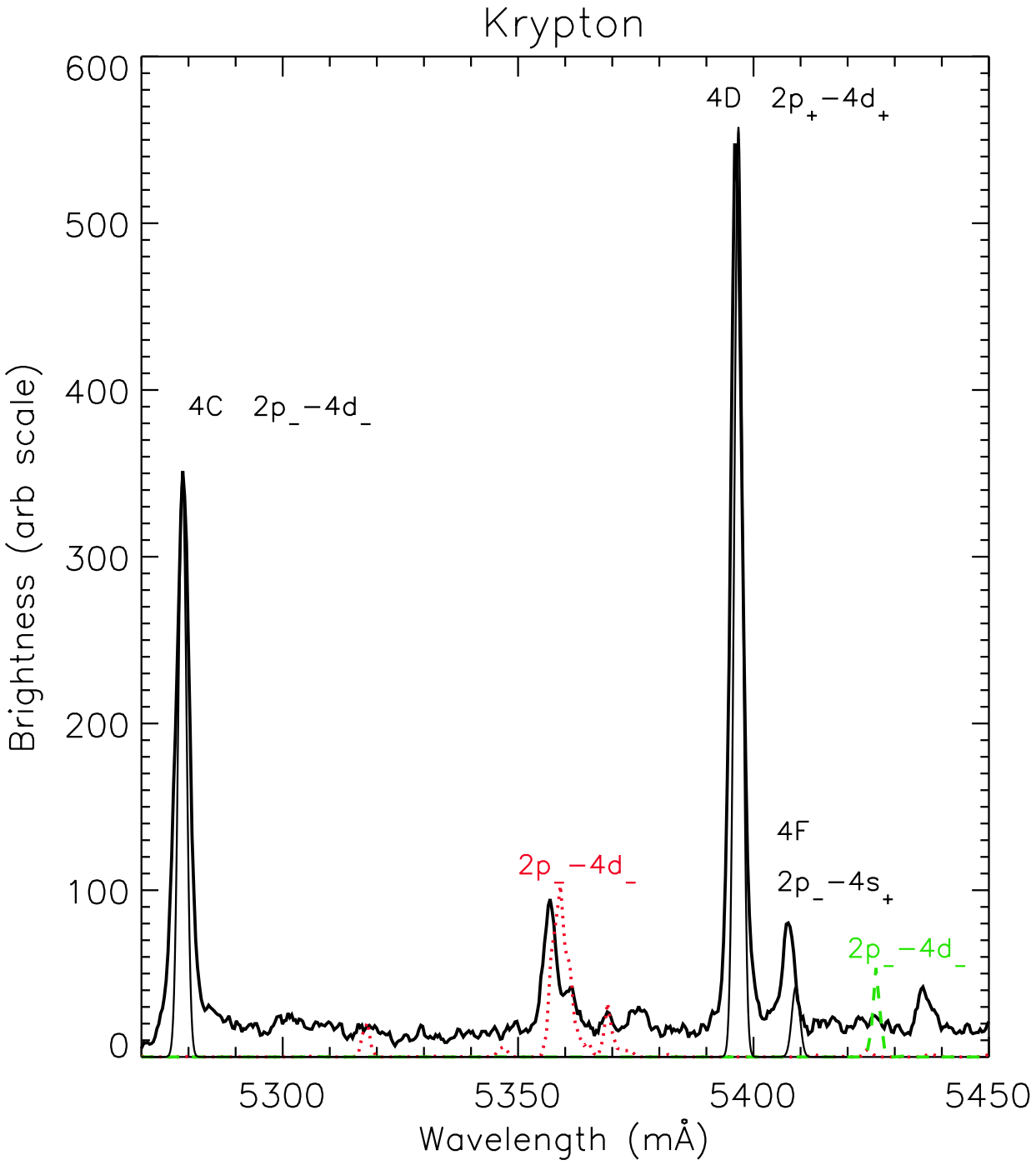
Krypton
600
500
400
300
200
100
0
Brightness (arb scale)
4C 2p_−4d_
4D 2p+−4d+
2p_−4d_
4F
2p_−4s+
2p_−4d_
5300
5350
5400
5450
Wavelength (mÅ)

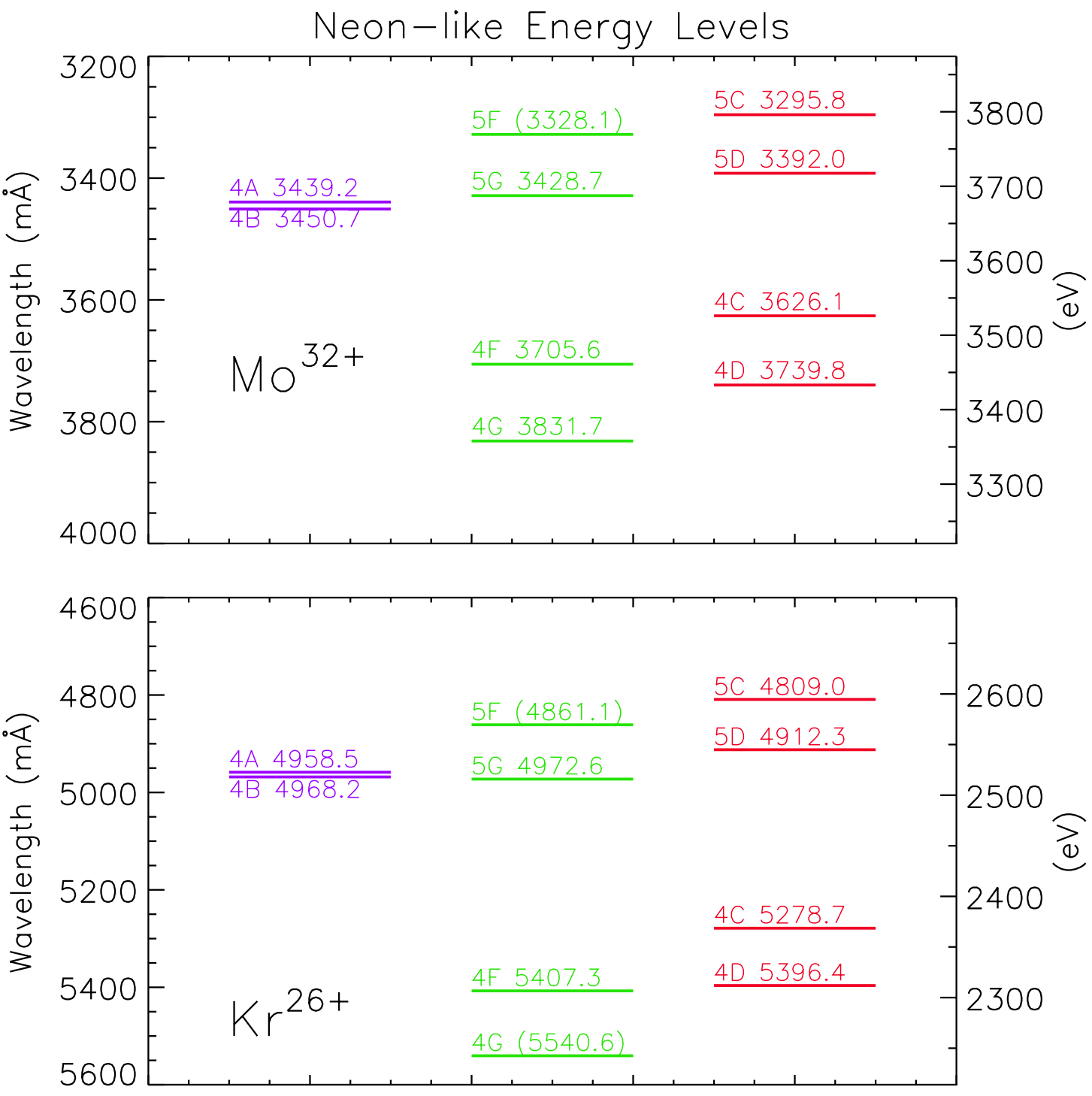
Neon−like Energy Levels
Wavelength (mÅ)
3200
3400
3600
3800
4000
3800
3700
3600
3500
3400
3300
(eV)
4A 3439.2
4B 3450.7
5F (3328.1)
5G 3428.7
4F 3705.6
4G 3831.7
5C 3295.8
5D 3392.0
4C 3626.1
4D 3739.8
Mo32+
Wavelength (mÅ)
4600
4800
5000
5200
5400
5600
2600
2500
2400
2300
(eV)
4A 4958.5
4B 4968.2
5F (4861.1)
5G 4972.6
4F 5407.3
4G (5540.6)
5C 4809.0
5D 4912.3
4C 5278.7
4D 5396.4
Kr26+

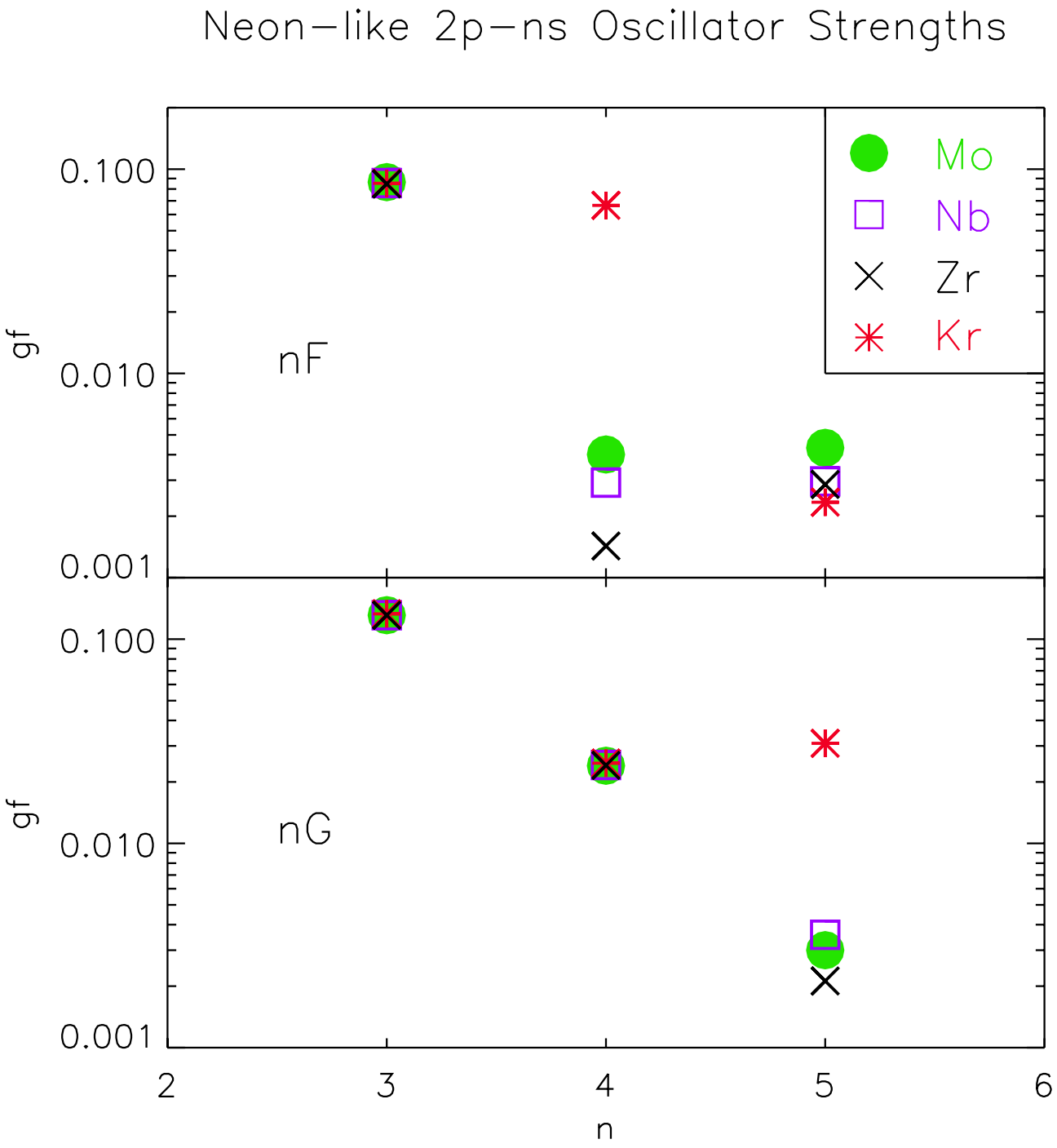
Neon−like 2p−ns Oscillator Strengths
Mo
Nb
Zr
Kr
nF
nG
gf
gf
0.100
0.010
0.001
0.100
0.010
0.001
2
3
4
5
6
n

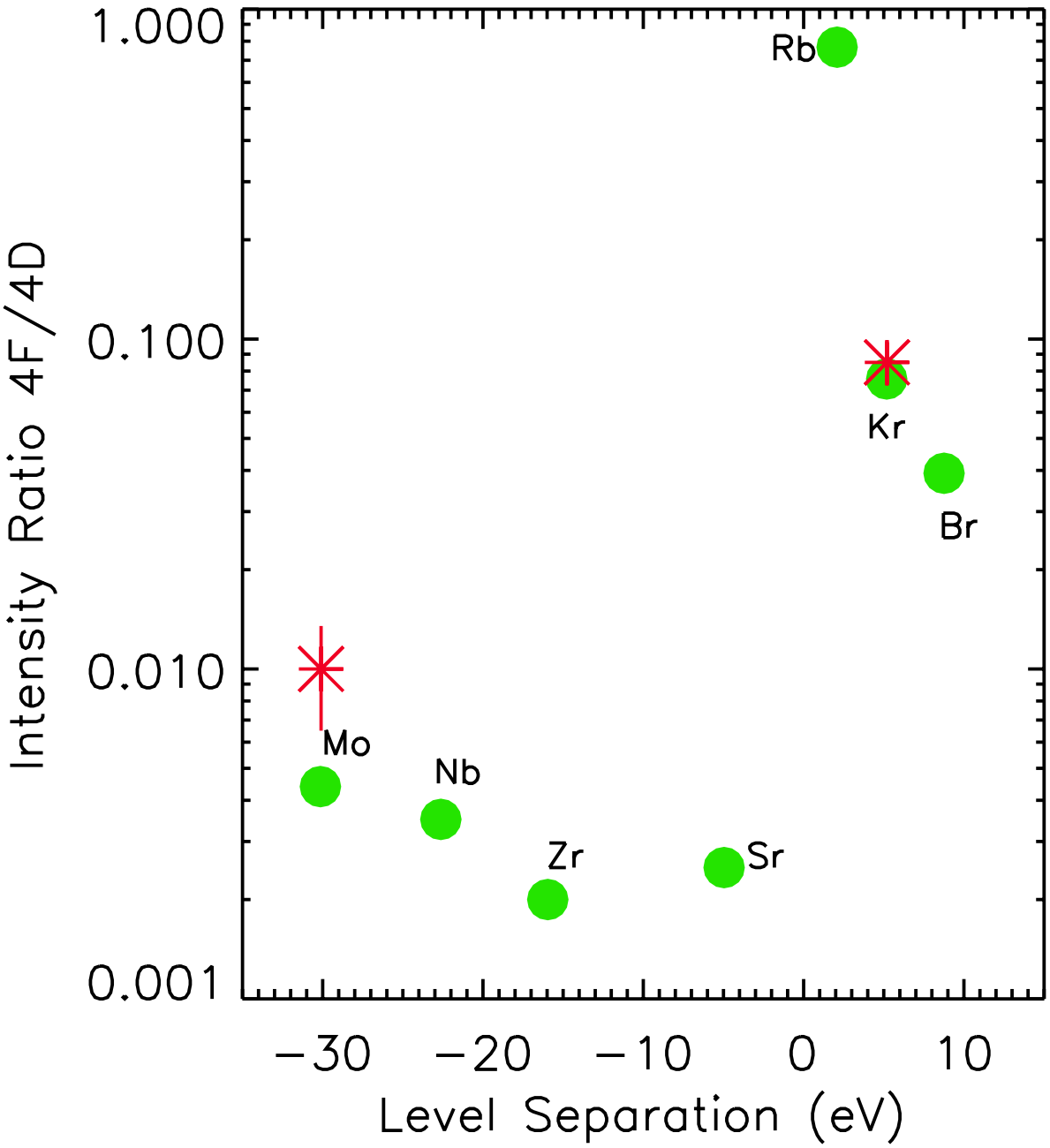
1.000
0.100
0.010
0.001
Intensity Ratio 4F/4D
Rb
Kr
Br
Mo
Nb
Zr
Sr
−30
−20
−10
0
10
Level Separation (eV)

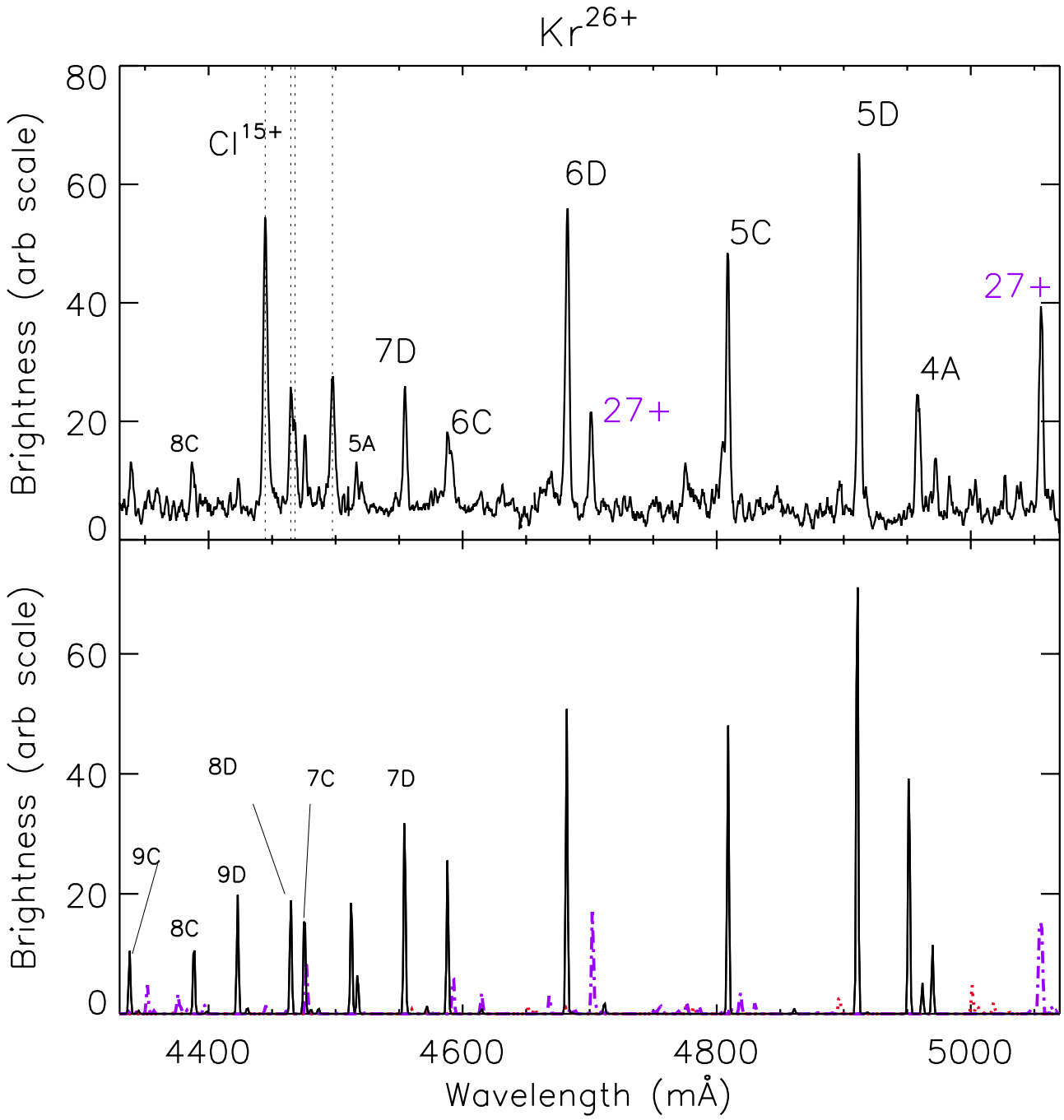
Kr26+
Cl15+
8C
5A
7D
6C
6D
27+
5C
5D
4A
27+
9C
8C
9D
8D
7C
7D
Brightness (arb scale)
Brightness (arb scale)
0
20
40
60
80
0
20
40
60
4400
4600
4800
5000
Wavelength (mÅ)

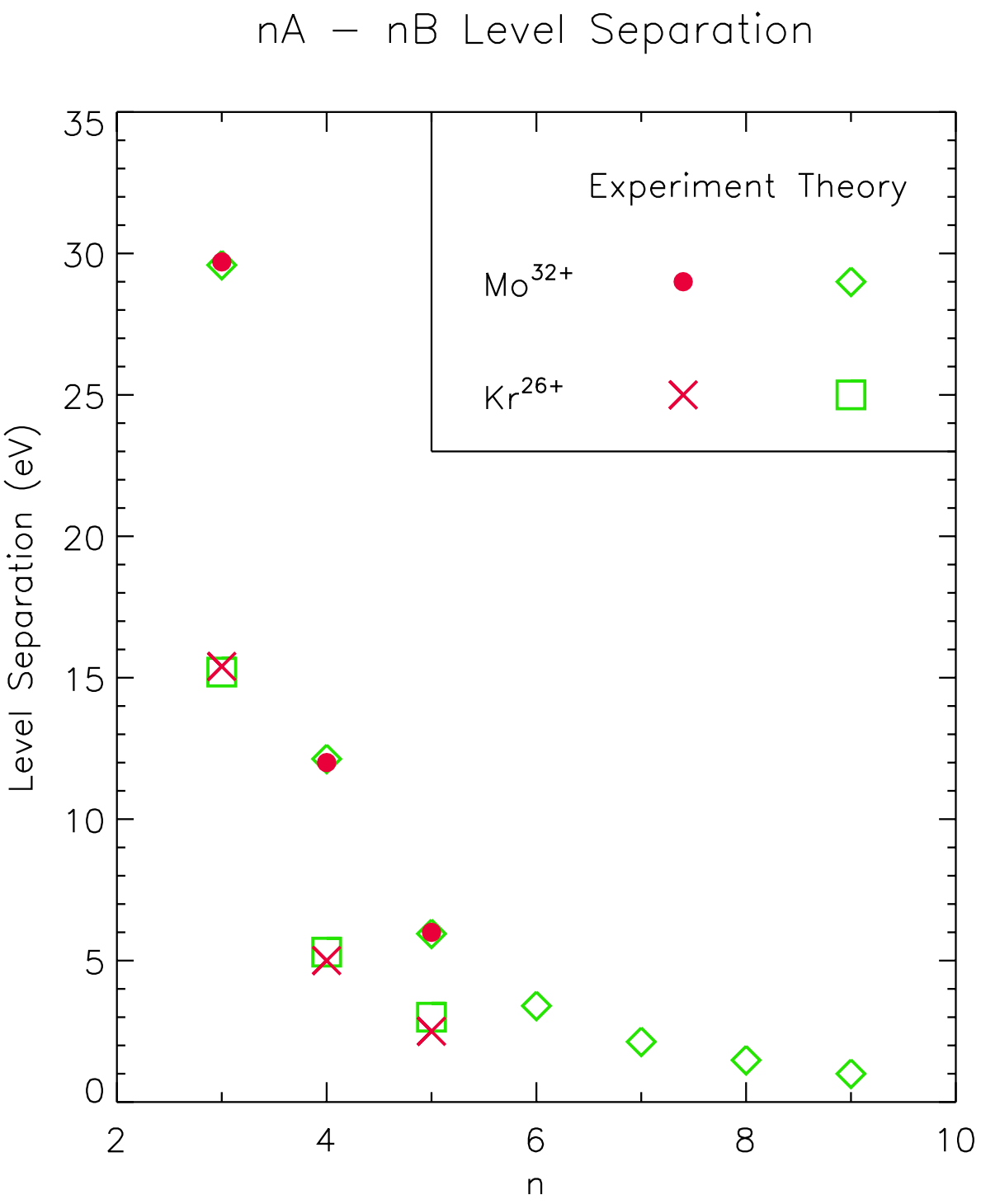
nA – nB Level Separation
Experiment Theory
Mo32+
Kr26+
Level Separation (eV)
n
0
5
10
15
20
25
30
35
2
4
6
8
10

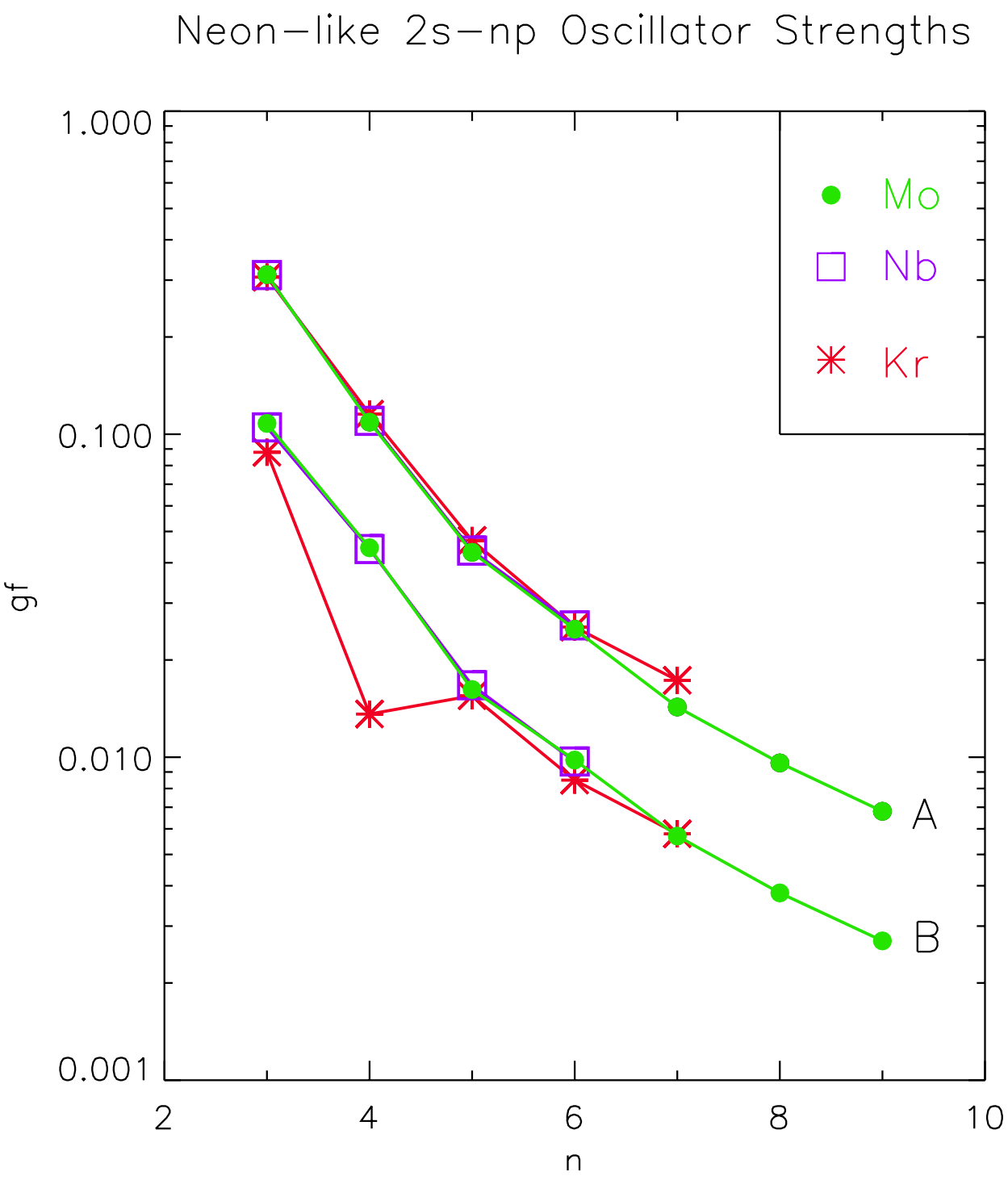
Neon−like 2s−np Oscillator Strengths
1.000
0.100
0.010
0.001
gf
2
4
6
8
10
n
Mo
Nb
Kr
A
B

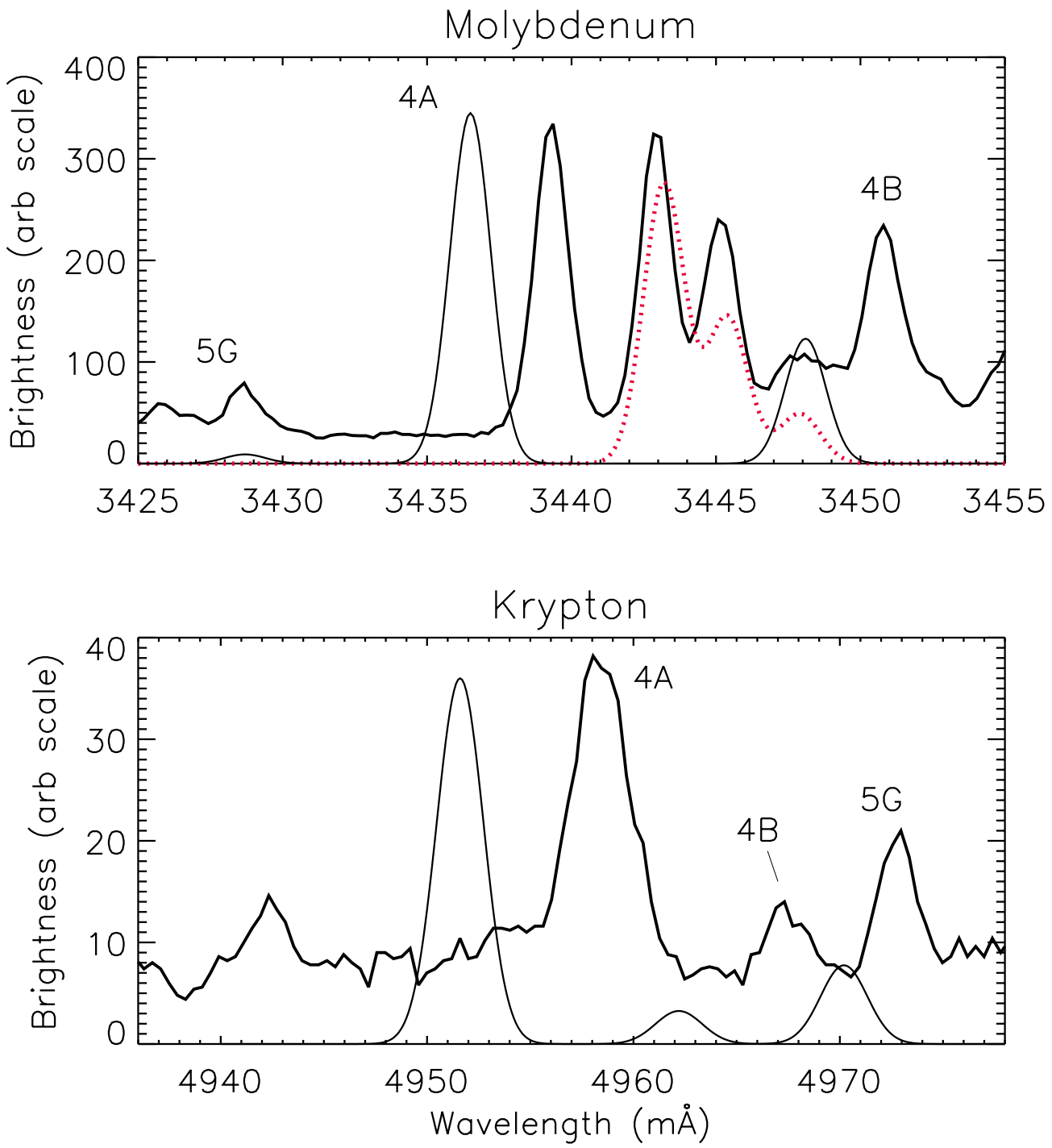
Molybdenum
Brightness (arb scale)
400
300
200
100
0
4A
4B
5G
3425
3430
3435
3440
3445
3450
3455
Krypton
Brightness (arb scale)
40
30
20
10
0
4A
4B
5G
4940
4950
4960
4970
Wavelength (mÅ)

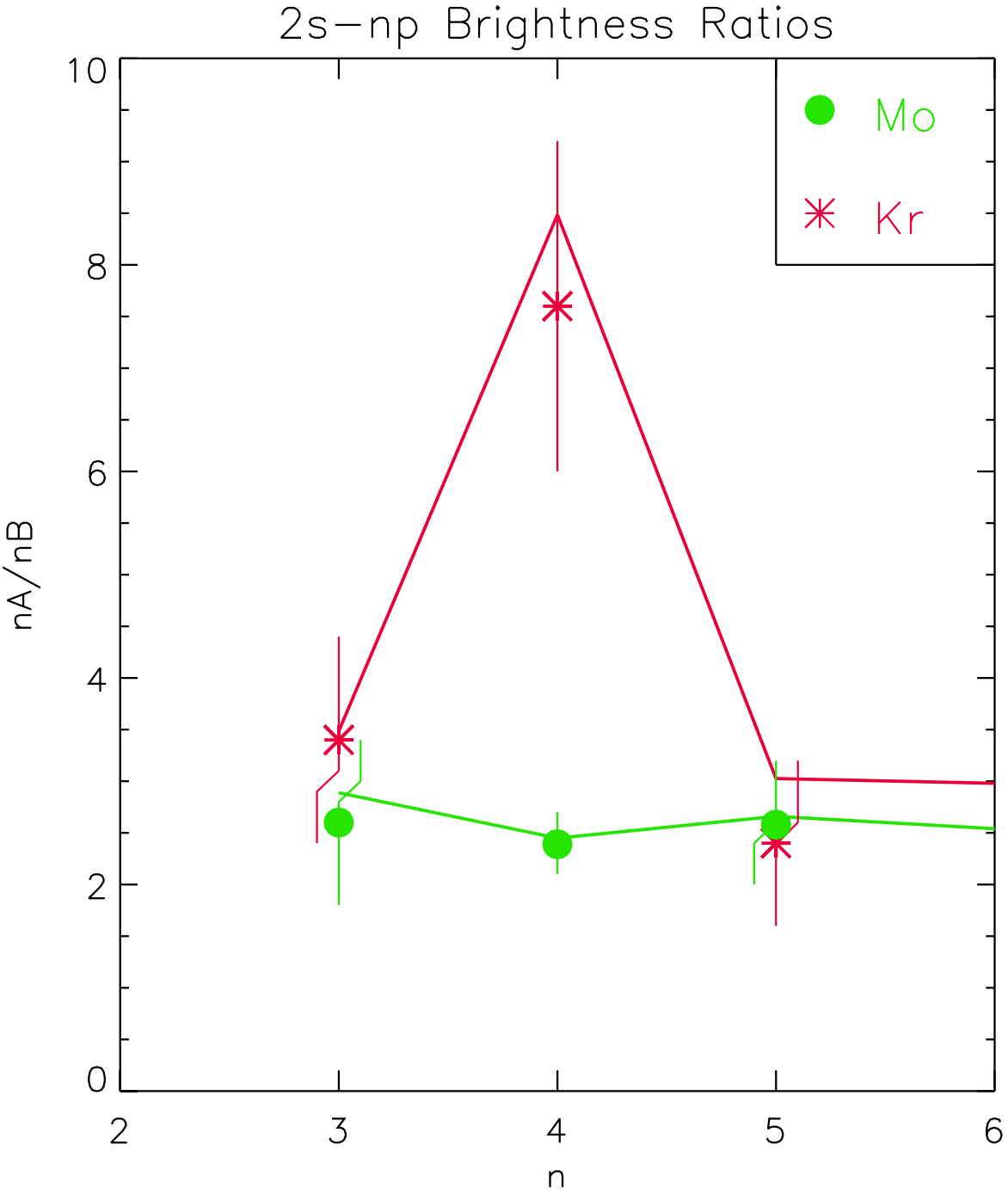
2s−np Brightness Ratios
Mo
Kr
nA/nB
n
0
2
4
6
8
10
2
3
4
5
6

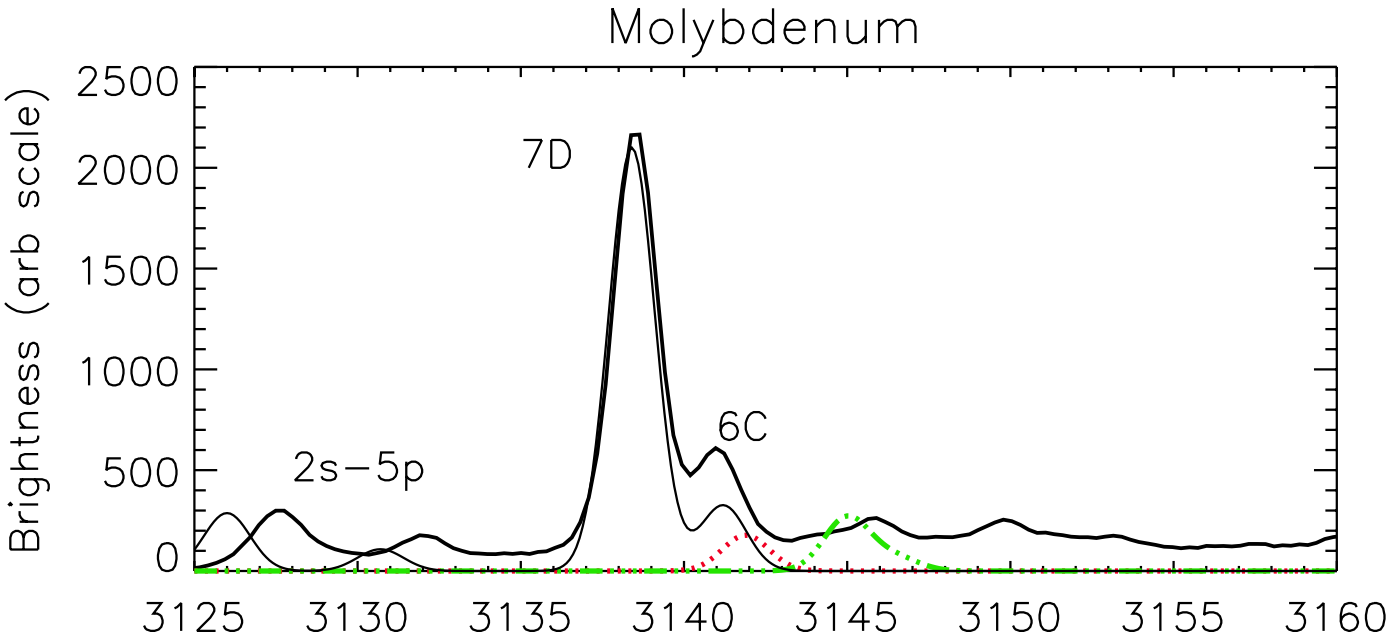
Molybdenum
Brightness (arb scale)
2500
2000
1500
1000
500
0
7D
6C
2s−5p
3125
3130
3135
3140
3145
3150
3155
3160

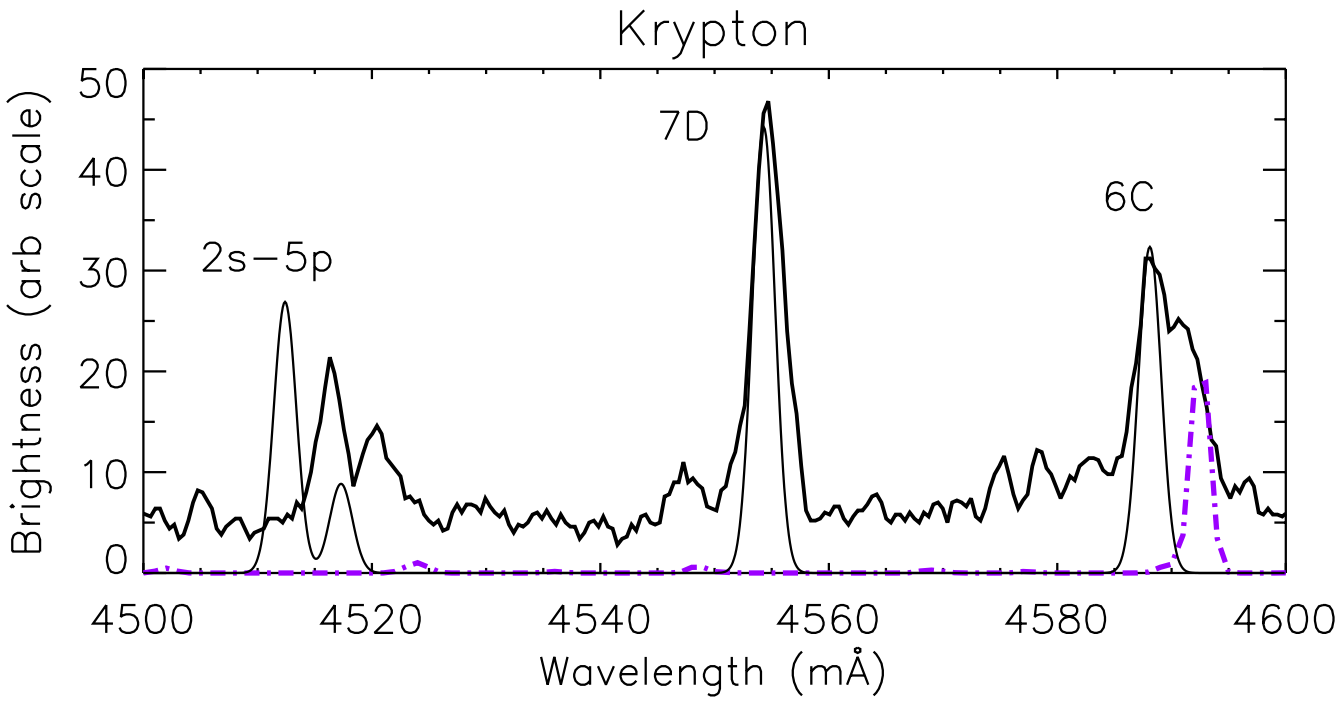
Krypton
Brightness (arb scale)
50
40
30
20
10
0
7D
6C
2s−5p
4500
4520
4540
4560
4580
4600
Wavelength (mÅ)

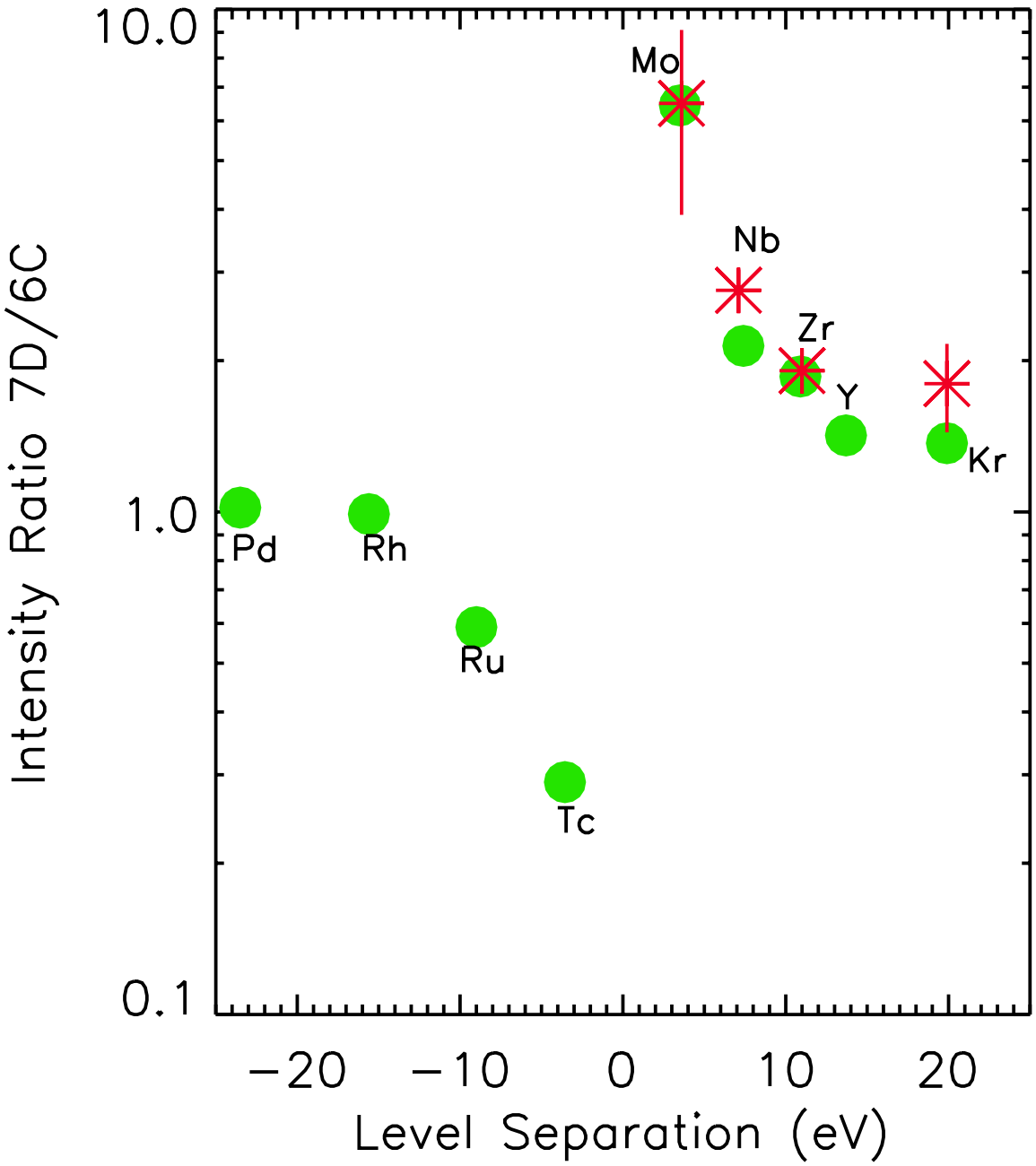
10.0
1.0
0.1
Intensity Ratio 7D/6C
Mo
Nb
Zr
Y
Kr
Pd
Rh
Ru
Tc
−20
−10
0
10
20
Level Separation (eV)

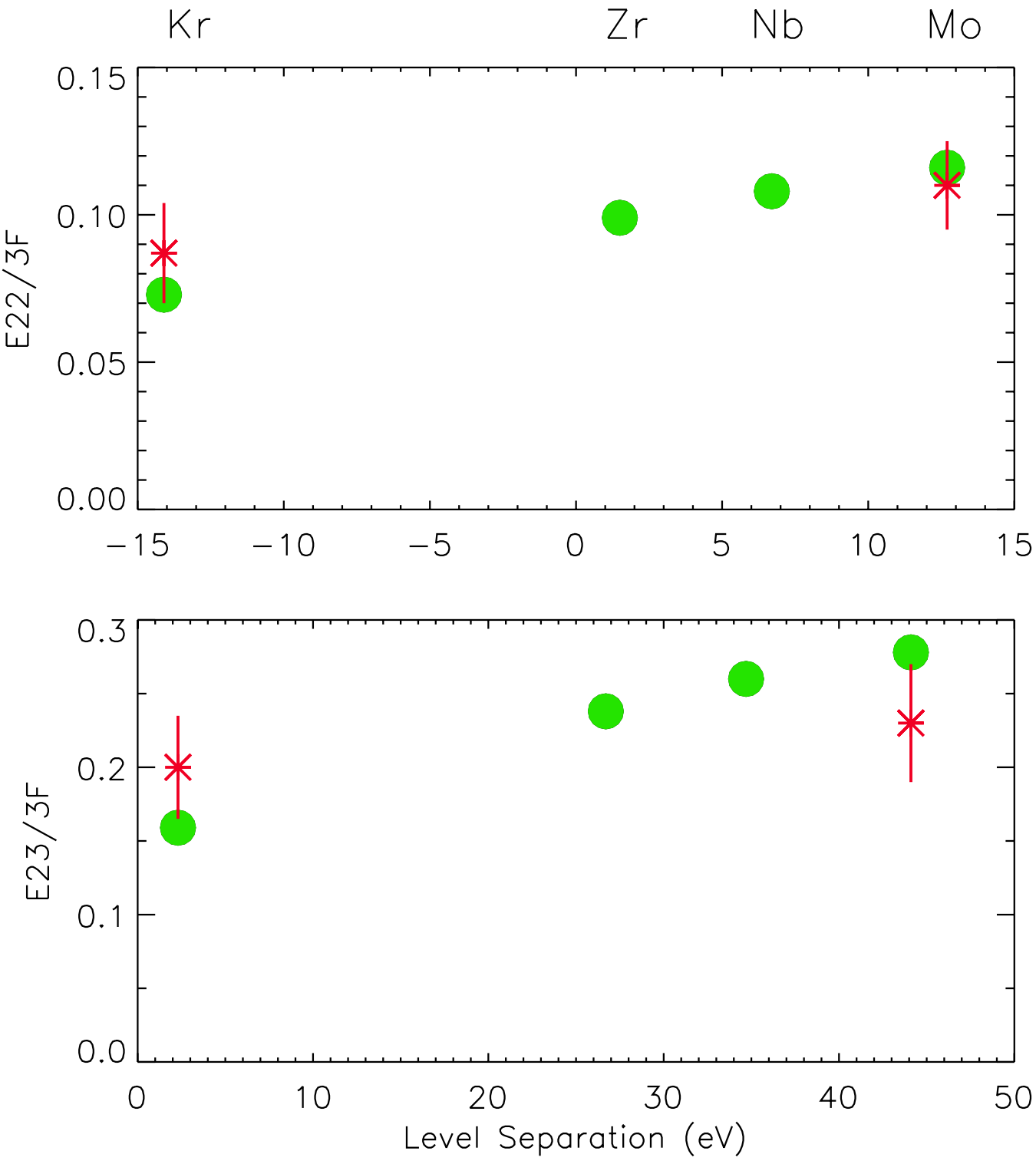
Kr
Zr
Nb
Mo
0.15
0.10
0.05
0.00
E22/3F
−15
−10
−5
0
5
10
15
0.3
0.2
0.1
0.0
E23/3F
0
10
20
30
40
50
Level Separation (eV)